INDONESIAN JOURNAL ON GEOSCIENCE
Geological Agency
Ministry of Energy and Mineral Resources

Journal homepage: http://ijog.geologi.esdm.go.id
ISSN 2355-9314, e-ISSN 2355-9306

Temporal Variations of Petrological Characteristics of Tangkil and Rajabasa Volcanic Rocks, Indonesia

Reza Firmansyah Hasibuan[1], Tsukasa Ohba[1], Mirzam Abdurrachman[2], and Takashi Hoshide[1]

[1]Graduate School of International Resource Sciences, Akita University, Akita 010-8502, Japan.
[2]Department of Geology, Institut Teknologi Bandung, Bandung 40132, Indonesia.

Corresponding author: reza.f.hasibuan@gmail.com
Manuscript received: August, 28, 2019; revised: December, 19, 2019;
approved: January, 09, 2019; available online: May, 11, 2020

Abstract - Tangkil and Rajabasa Volcanoes are neighbouring subduction-zone volcanoes located on the southeast tip of Sumatra Island (Sunda Strait, Indonesia). Stratigraphic correlation of lavas in Tangkil-Rajabasa volcanic area was established from field observations, morphological analysis, and K-Ar dating analysis. Detailed petrography and geochemical data of two and eleven lava units from Tangkil and Rajabasa, respectively, were then integrated with the stratigraphy to show the temporal variations. Early stage (> 4.3 Ma) effusives of Tangkil Volcano are dacitic to rhyolitic (67-71 wt. % SiO_2; Tklf), whereas the later (*c.* 4.3 Ma) rocks are basalt to basaltic andesite (*c.* 52 wt. % SiO_2; Tklm). Tangkil shows bimodal magmatism, of which the felsic endmember is > 71 wt. % SiO_2 and < 0.1 wt. % MgO. Lavas of Rajabasa Volcano are comparatively younger (*c.* 0.3 to 0.1 Ma) with compositions ranging from basalt to andesite (51-62 wt. % SiO_2; Rbs). Chemical variations of Rajabasa accounts for the interactions of at least three endmembers: Mg-rich medium-K basalt magma, low-Mg medium-K basalt magma, and high-K andesitic magma. During the long evolution of Rbs magma system, the temporal chemistry shows rising-falling variation in SiO_2 and MgO indicating the three magmas were active. The felsic endmember magma of Rajabasa is fixed in composition (at ~62 wt. % SiO_2; ~2.2 wt. % MgO). The rocks from the last Tklf and Rbs indicate open system processes by containing plagioclase and pyroxene phenocrysts that show resorption of evolved core and overgrowth of less evolved mantle. The multiple zones of dissolution-overgrowth in plagioclase crystals and the fluctuating trend in temporal whole-rock variation suggest that the changes of magmatic condition in temperature, H_2O, or chemical composition were repetitive.

Keywords: temporal variation, evolution, magma recharge, Rajabasa, Tangkil, Sunda Strait

How to cite this article:
Hasibuan, R.F., Ohba, T., Abdurrachman, M., and Hoshide, T., 2020. Temporal Variations of Petrological Characteristics of Tangkil and Rajabasa Volcanic Rocks, Indonesia. *Indonesian Journal on Geoscience*, 7 (2), p.135-159. DOI: 10.17014/ijog.7.2.135-159

Introduction

Temporal chemical variations of volcanic rocks from subduction-related volcanoes have been documented in the past decades (*e.g.* Newhall, 1979; Tsukui, 1985; Camus *et al*., 1987; Prosser and Carr, 1987; Gertisser and Keller, 2000, 2003; Amma-Miyasaka and Nakagawa, 2003; Wibowo, 2017) by integrating the stratigraphy, isotopic dating, and whole-rock chemistry to understand the magmatic evolution. The temporal variations are detected at various time scales, ranging from inhomogeneous volcanic products by a single eruption in minutes or hours to variations during a series of eruptions in thousands of years; or even the entire lifetimes of a volcano or volcanic field, up to tens of million years. The variations in many calc-alkaline volcanic rocks

are accounted for by periodic influxes of mafic magma to shallow felsic magmas (*e.g*. Newhall, 1979 for Mayon, Philippines; Tsukui, 1985 for Daisen, Japan; Camus *et al*., 1987 for Krakatau, Indonesia; Prosser and Carr, 1987 for Poás Volcano, Costa Rica; Gertisser and Keller, 2000, 2003 for Merapi, Indonesia; Amma-Miyasaka and Nakagawa, 2003 for Miyake-Jima, Izu-Mariana Arc; Toya *et al*., 2005 for Aoso, Japan; Wibowo, 2017 for Sundoro, Indonesia). In previous studies, the evolution of magma systems was mostly discussed on the basis of temporal variations in the whole-rock chemistry with phenocryst mineral chemistry (*e.g.* Borgia *et al*., 1988; Amma-Miyasaka and Nakagawa, 2003; Takahashi and Nakagawa, 2015). Not all were understood by thorough observation of textures, zoning patterns, and assemblages of minerals with temporal chemical variation (*e.g*. Humphreys *et al*., 2006, Higgins *et al*., 2015). In many Sunda Arc Volcanoes, magmatic evolutions have been discussed based on mineral and the whole-rock chemistry (*e.g.* Foden, 1983; Reubi and Nicholls, 2004; Gardner *et al*., 2012; Dempsey, 2013; Innocenti *et al*., 2013; Métrich *et al*., 2017), whereas detailed investigations based on mineral textures are limited (Carn and Pyle, 2001; Wibowo, 2017).

This work is a case study to investigate the temporal petrologic variations, including the whole-rock chemistry and petrography in volcanoes that are not well studied like Tangkil and Rajabasa Volcanoes in Sumatra. No historical eruptions were recorded on both volcanoes. Nazarwin (1994) and Suswati *et al*. (2001) have conducted geological mapping of Rajabasa Volcano on the basis of field observation and remote sensing. Andi Mangga *et al.* (1994) and Barber *et al.* (2005) reported that Tangkil and Rajabasa Volcanoes are characterized by andesitic volcanic centres. On the other hand, Bronto *et al.* (2012) reported that Rajabasa Volcano erupted basaltic to andesitic lava flows, and they established the evolution model of Rajabasa Volcano based on the remote sensing analysis and field geologic work. Bronto *et al.* (2012), however, did not carry out detailed petrographic works, and the stratigraphic variation of petrological characteristics has not been discussed. Therefore, the chronological evolution of the magma system was not clear. To understand the evolution, age determination of the lava units and detailed petrological study are necessary. The temporal variations are important to clarify the evolution of magmas beneath Tangkil and Rajabasa.

This study aims to provide new insights on the volcanic history and magma evolution of Tangkil and Rajabasa Volcanoes. The lava stratigraphy is established by field observations and geomorphological analysis, supplemented by K-Ar ages. New data of the whole-rock major and minor elements are also presented for rocks from both volcanoes. The approach involves the description of petrological variations by a careful observation on mineral textures, zoning patterns, and mineral assemblages, and they are discussed on the basis of temporal geochemical data. The stratigraphy, whole-rock chemistry, and petrography data presented in this study are directed to investigate a temporal petrological variation. In addition, the observations on mineralogy help to identify the magmatic processes in which the minerals have been through during the evolution of the magma system. Modeling of major elements with MELTS calculation (Ghiorso and Sack, 1995; Gualda *et al*., 2012) was also carried out.

Geotectonic Setting and Geological Background

Currently, the Indo-Australian Oceanic Plate is subducting beneath the Eurasian Continental Plate with a convergence rate of 6 - 7 cm a^{-1} (McCaffrey, 1991; Hall, 2009). This activity has formed a volcanic arc, namely the Sunda Arc, stretching over 5,600 km from the Andaman Islands to Banda Arc. The Sunda Strait is a transitional zone between the Java perpendicular and Sumatra oblique subductions (*e.g*. Huchon and Le Pichon, 1984; Malod *et al*., 1995; Barber *et al.,* 2005). A volcanic alignment across the Sunda Strait runs through from Panaitan Island, via Krakatau Island, the Sebesi and Sebuku Islands, Tangkil and Rajabasa Volcanoes, to the Sukadana basalt plateau from SSW to NNE (Figure1). Tangkil and Raja-

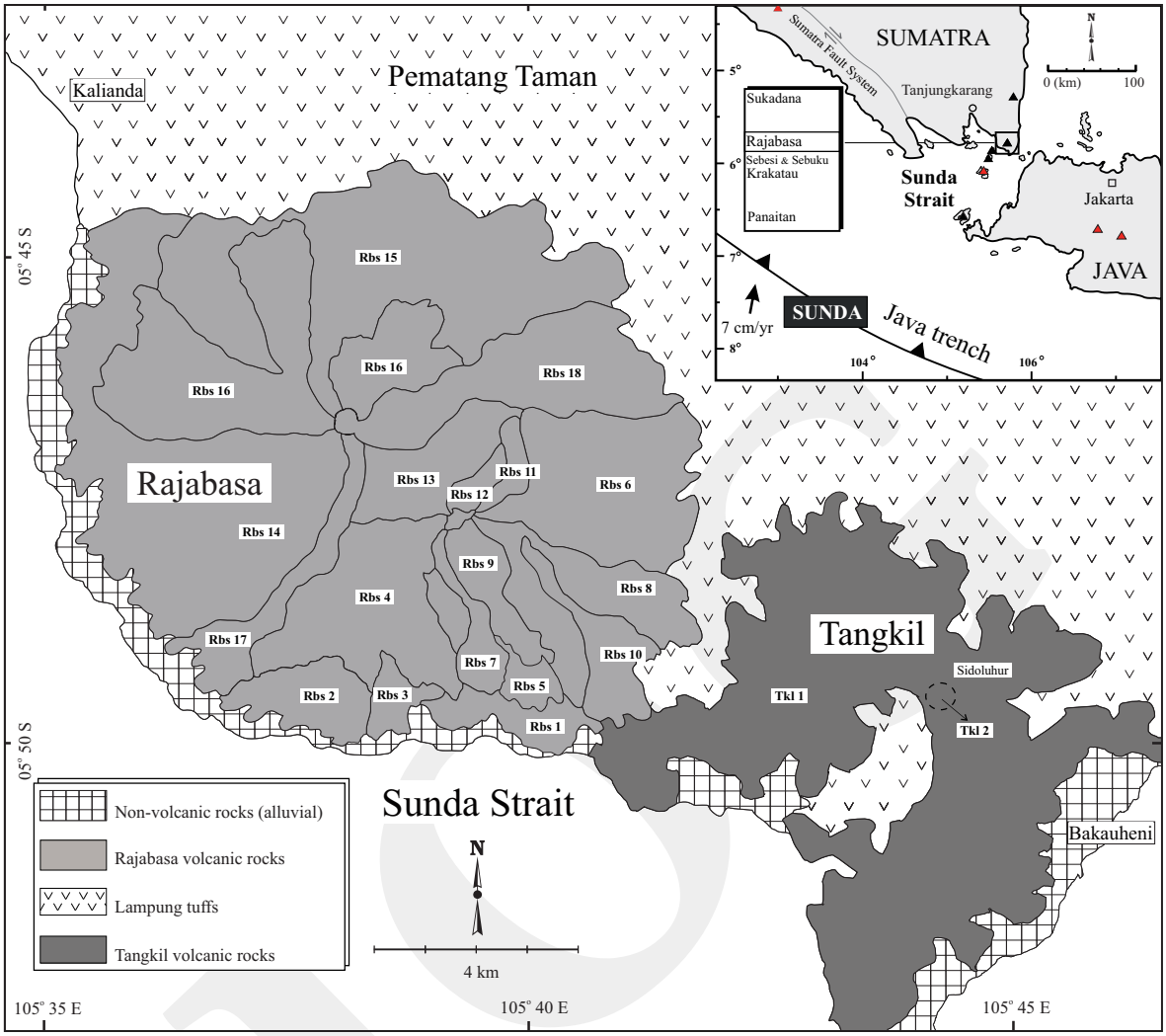

Figure 1. Geologic map displaying the distribution of Tangkil and Rajabasa unit lavas. The inset map shows the location of the volcanoes in Sunda Strait region.

basa Volcanoes are neighbours, where Rajabasa Volcano is adjacent to Tangkil Volcano to NW.

The Sunda Strait is tectonically complex (*e.g.* Ninkovich, 1976). In addition to the N−S compressional force related to the subduction in the southern regime, the strait has undergone an extension as a result of the clockwise rotation of Sumatra relative to Java since Late Cenozoic (Nishimura *et al.*, 1986; Harjono *et al.*, 1991). The Sumatra Fault System (Semangko) is a major strike-slip dextral fault zone that extends NW−SE from Andaman Sea to Sunda Strait (*e.g.* Barber *et al.*, 2005). In addition to the slab subduction in the southern margin, the volcanism of Tangkil and Rajabasa Volcanoes might have been affected by this complex tectonic setting.

There is no detailed geologic study regarding volcanic activities in Tangkil Volcano yet as the original lava geomorphology has been lost by erosion. In the geological map by Andi Mangga *et al.* (1994), Tangkil volcanic products are described as the Tertiary andesite lava (Tpv). The volcanic products from Tangkil Volcano are distributed from the southeast of Rajabasa Volcano to the Bakauheni seaport in the southeast. The deposits from Tangkil Volcano are overlain by later pyroclastic fall deposits, which are named as Lampung tuffs (Bemmelen, 1949; Andi Mangga *et al.*, 1994). According to Nishimura (1980) and Nishimura *et al.* (1984, 1986), Lampung tuffs were spewed at the southern end of Semangko fault at 1 ± 0.2 Ma to 0.09 ± 0.01 Ma.

Lava morphology is well preserved on Rajabasa Volcano so that studies of lava stratigraphy can be established by observing the overlapping lava morphologies. Andi Mangga *et al*. (1994) described Rajabasa Volcano as Young Volcanic Deposits (Qhv), dominated by andesite-basalt lava. Volcanic rocks of Rajabasa overlie the Lampung Tuffs. Bronto *et al.* (2012) established the evolution of Rajabasa Volcano as follows: construction of the pre-Rajabasa composite cone, destruction of the pre-Rajabasa cone by a huge eruption leaving the 25 km-diameter pre-Rajabasa caldera (Figure 2), and the construction of the Rajabasa cone inside the pre-Rajabasa caldera. The volcanic rocks of pre-Rajabasa cone are not exposed because of erosion. The ridge of pre-Rajabasa caldera, however, can be recognized on *c.* 5 km outward from the northern and eastern base of Rajabasa Volcano by an arc-shaped ridge (Figure 2). All the existing lava inside the ridge belongs to Rajabasa Volcano formed after the collapse of pre-Rajabasa caldera.

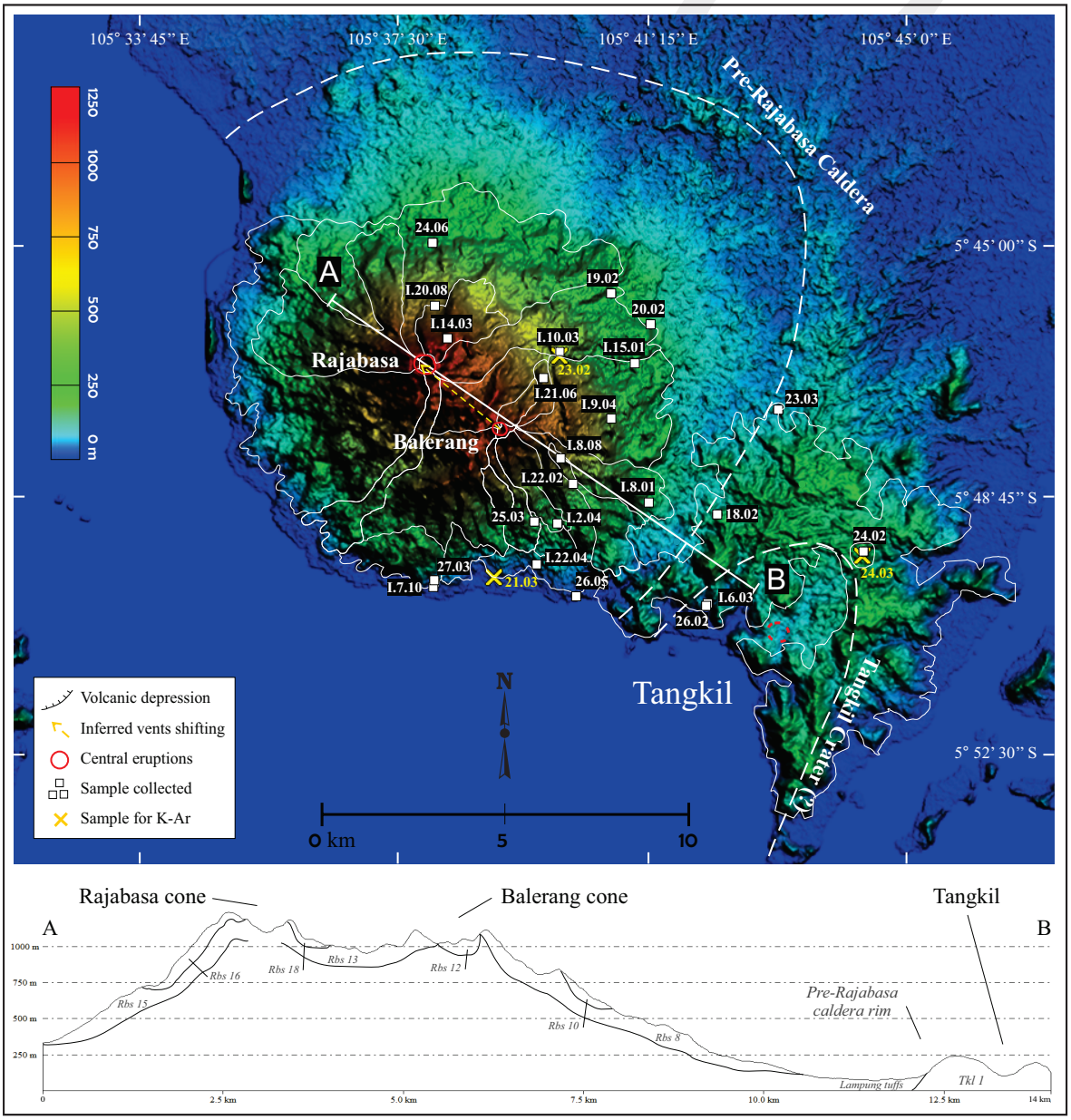

Figure 2. ASTER image displaying Rajabasa Volcano inside the caldera, as well as the NW trend of vents position from Tangkil to Rajabasa. The lower figure is the topographic cross section in this volcanic region, exhibiting the peaks.

Samples and analytical methods

A morphological analysis of Rajabasa Volcano was carried out on the basis of the digital elevation model and satellite image. This analysis was done to determine the stratigraphic correlation of lava units. Here, Light Detection and Ranging (LiDAR; only available for Rajabasa Volcano) and Advanced Spaceborne Thermal Emission and Reflection Radiometer (ASTER) data were used to delineate each eruptive/flow unit, lineaments, and areal morphology by utilizing Geographic Information System (GIS) 10 and Global Mapper ver. 15 software. The LiDAR data was obtained from Hasibuan (2014) and DEM (ASTER) data is an open access provided by the U.S. Department of Interior, USGS. The DEM describes the topography of Tangkil and Rajabasa which appeared as interpolation of contour lines. This analysis can provide the recognition and localization of the main volcanic features (*e.g.* Norini *et al*., 2004). As lava lobe geomorphology is well preserved, the sequence of lava was established based on the geomorphological analysis, as well as the relationship observed at exposures. Field observation is an important stage to ascertain order from morphological analysis.

In this study, the total of twenty lava samples were collected from Rajabasa and five lava and one dyke samples from Tangkil. The sampling covers two units from Tangkil Volcano and eleven units from Rajabasa Volcano. The exposure of fresh volcanic rocks is limited by thick vegetation. For this reason, some lava units from Rajabasa Volcano were not able to be sampled (Rbs 3, Rbs 4, Rbs 5, Rbs 12, Rbs 13, Rbs 14, and Rbs 17). Thin sections and rock powder were prepared from each sample for the petrography and whole-rock chemical analysis. Polished thin sections were also prepared for SEM-EDS analysis.

Three lava samples were selected for K-Ar isotope dating; one basaltic lava sample from Tangkil Volcano (sample 24.03), and two andesitic lava samples from the youngest and oldest lava flow units of Rajabasa Volcano (samples 21.03 and 23.02). These samples are representative to constraint the lifespan of the volcanoes. The analysis was carried out at Hiruzen Institute for Geology and Chronology Corp., Okayama, Japan. K-Ar determinations were made using crushed groundmass. The argon contents were analyzed with a single collector by an isotopic dilution method using an argon 38 spike. The errors for the obtained gas are at the two-sigma confidence level. In detail, this analysis refers to Yagi (2006) for sample preparation, Nagao *et al.* (1984) for potassium analysis, and Itaya *et al*. (1991); Nagao and Itaya (1988); Nier (1950); Steiger and Jäger (1977) for the argon isotope analysis.

The whole-rock chemical compositions were determined with X-ray fluorescence analysis (ZSX Primus II, Rigaku Co. installed at Akita University) using the glass bead method. The powder samples were prepared by grinding in an agate mill. To determine the LOI, the powder samples were furnaced at 900ºC. The dilution ratio of glass bead is 1:5 (rock: flux of a mixture of $Li_2B_4O_7$ and $LiBO_2$). After grinding the mixtures using an agate mortar and pestle, they were fused at 1,150°C to make glass beads. The compositions of ten major elements (Si, Ti, Al, Fe, Mn, Mg, Ca, Na, K, and P) and nine minor elements (Ba, Zr, Rb, Sr, Nb, Cr, Ni, Y, and V) were determined by matrix-corrected calibration curves obtained from the measurements of fifteen samples of GSJ (Geological Survey of Japan) Igneous Rock Series.

Back-scattered electron images (BSEI) were captured with the scanning electron microscope (SEM: JSM-6610LV, JEOL Co.) and line-scanning analysis of individual minerals were carried out using energy-dispersive X-ray spectroscopy (EDS: INCA X-act, Oxford Instruments) at Akita University. The conditions of this analysis were set at: an acceleration voltage of 15 kV, a probe current of 2.2 nA, and working distance of 10 mm.

Results

Geology of Tangkil and Rajabasa Volcanoes

The volcanic centres of Tangkil and Rajabasa Volcanoes are aligned along a SE - NW direction, over a distance of *c.* 11 km. The boundary

between Tangkil volcanic products and Rajabasa volcanic products is located on the flat plain along the northwestern base of Tangkil Volcano (Semanak Village) where the Lampung tuffs are distributed. Lampung tuffs overlie the volcanic products of Tangkil and are overlain by the volcanic products of Rajabasa.

Tangkil and Rajabasa Volcanoes have different degrees of erosion. Tangkil Volcano has lost its original morphology and thus it is regarded as the remnant of an old volcanic edifice (Figure 2). Based on DEM observation, the geomorphology of the volcano is a hill with slopes of 5° to 35°. Tangkil Volcano is originally a composite volcano that consists of lava and lahar deposits. Rajabasa Volcano is a steep-sided volcano with radial slopes of more than 20°. Rajabasa Volcano is also a composite volcano, composed of dominant lava, tuff, volcanic breccia, and lahar deposits . Rajabasa Volcano consists of two main volcanic cones (Figure 2): Rajabasa cone and Balerang cone. The younger eruption centre of Rajabasa cone is located in the NW of the older eruption centre of Balerang cone. Bronto *et al*. (2012) suggested the two volcanic cones were formed by the movement of eruption centres from SE to NW. Two horseshoe-shaped depressions on the northern and western flanks of the Balerang cone indicate the occurrence of sector collapses or landslides.

The lava stratigraphy of Tangkil and Rajabasa Volcanoes is shown in Figure 3. Tkl 1 from Tangkil Volcano is the oldest unit in the area, which

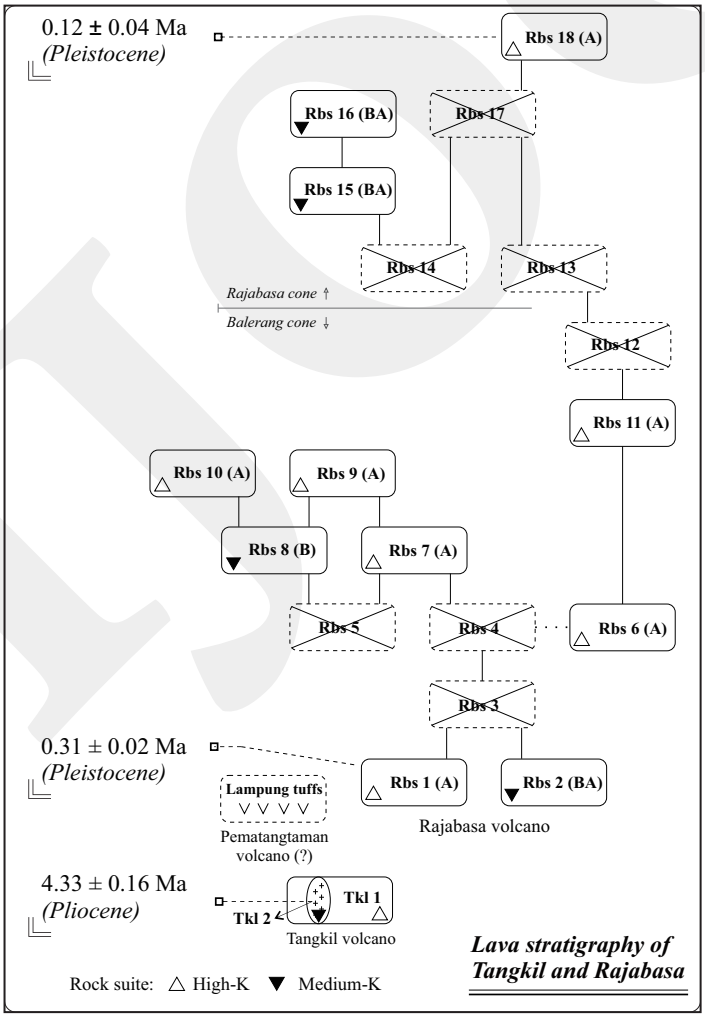

Figure 3. Lava stratigraphy of Tangkil and Rajabasa Volcanoes. B, Basalt; BA, Basaltic andesite; A, Andesite. The ages are shown for three lava units, in which Tangkil is an older volcano than Rajabasa. The crossed marks indicate the absence of data, caused by the difficult access, the intense alteration, or the volcanic products other than effusive lava flow or intrusion.

was later overlain by Tkl 2. The Tkl 1 is occupied by dacite lava. On the other hand, the Tkl 2 is occupied by basaltic rocks. The deposits of Tangkil Volcano were overlain by Lampung tuffs. The earliest lavas of Rajabasa, Rbs 1 and Rbs 2, overlie the Lampung Tuffs. There are some units drawn in a parallel age, because the stratigraphic orders of which another unit overlies the direct contact cannot be determined (Rbs 1 and Rbs 2, Rbs 7 and Rbs 8, Rbs 9 and Rbs 10) and they are regarded as concurrent products. The lava in the southern and eastern flanks of Rajabasa Volcano (Rbs 1 up to Rbs 12) was derived from the central vent of the Balerang cone. The lava units from the Balerang cone are dominated by andesite, accompanying minor basaltic andesite (Rbs 8) and basalt (Rbs 2) lavas. On the other hand, the basaltic andesite and andesite lavas on the northern and western flanks (Rbs 13 up to Rbs 18) were derived from the younger central vent of Rajabasa cone. The youngest andesite lava (Rbs 18) flowed to the eastern flank, into the horseshoe-shaped depressions of the older volcanic cone.

Field occurrences of the volcanic rocks from Tangkil and Rajabasa are lava, scoria deposit, and dyke. The volcanic rocks of Tangkil are widely distributed in Bakauheni and dominated by dacitic to rhyolitic lavas. The lavas are mostly blocky, and cooling joints (platy and columnar) are distinct in some lava units. All the lavas are more than 6 m thick. The felsic rocks are light grey in colour and show porphyritic to aphanitic glassy textures. The basaltic rocks (Tkl 2 in Figure 3) occur as strombolian scoria deposit and dyke that intruded the dacitic lava (Tkl 1 in Figure 3). In contrast to the felsic rocks, the basaltic rocks are distributed locally in Sidoluhur Village. Scoria deposit and dyke have the thickness of more than 15 m and 30 m, respectively. The scoria clasts are brownish and vesicular. On the other hand, the volcanic rocks of Rajabasa are dominated by basaltic andesite to andesite lavas. Most of the lavas are massive and dense, and some are autobrecciated and vesicular on the exterior. The thickness of the lavas ranges from a few meters to more than 50 m. The lavas are all porphyritic and have similar characteristics in groundmass colour and phenocryst size but varying in phenocryst assemblages. The rocks are light to dark grey in colour and contain phenocrysts with up to 4.3 mm in size. Variations of phenocryst assemblages are described further in the petrography section.

K-Ar Analysis

The results of K-Ar dating are shown in Table 1. The K-Ar age of the basalt from unit Tkl 2 of Tangkil Volcano (sample 24.03 in Table 1) is *c.* 4.3 Ma (Pliocene). Samples from the oldest (Rbs 1) and the youngest (Rbs 18) lava units from Rajabasa Volcano (21.03 and 23.02 in Table 1) were dated at *c.* 0.3 and *c*. 0.1 Ma, respectively. The result indicates that Rajabasa Volcano is as young as Late Pleistocene.

Table 1. Result of K-Ar age Measurement with an Error of 2% for Potassium Analysis (more than 0.2 wt %)

Sample No. (rock type)	Mineral (mesh size)	K content (wt.%)	Rad. ^{40}Ar (10^{-8}cc STP/g)	Non-rad. ^{40}Ar (%)	K-Ar age (Ma)	Age
23.02 (andesite)	groundmass (#60-80)	2.273 ± 0.045	1.07 ± 0.38	95.6	**0.12 ± 0.04**	Late Pleistocene
21.03 (andesite)	groundmass (#60-80)	2.664 ± 0.053	3.16 ± 0.15	70.6	**0.31 ± 0.02**	Late Pleistocene
24.03 (basalt)	groundmass (#60-80)	0.782 ± 0.016	13.16 ± 0.41	61.3	**4.33 ± 0.16**	Pliocene

Note: Sample no. 24.03 is representative for Tangkil Volcano, while sample no. 21.03 and 23.02 were collected from Rajabasa Volcano. The term of "rad.^{40}Ar", "nonrad.^{40}Ar", and "STP" states for radiogenic ^{40}Ar, nonradiogenic ^{40}Ar (atmospheric ^{40}Ar), and conditions of 0^{o}C and 1 atm, respectively.

Petrography

Most of the volcanic rocks from Tangkil and Rajabasa contain phenocrysts of plagioclase, clinopyroxene, orthopyroxene, and opaque minerals, with additional phenocrysts of olivine, spinel, hornblende, or biotite. Spinel occurs only in rocks from Rajabasa Volcano. Aggregates of plagioclase + pyroxene + opaque are common in all samples except in Tkl 2. All the samples are porphyritic, and phenocrysts in mafic samples are more abundant. The groundmass textures are homogeneous and mostly consist of plagioclase, fine-grained pyroxene, apatite, opaque minerals, and glass. Lavas from the felsic Tangkil (sample 23.03 from Tkl 1) and Rajabasa Volcanoes contain plagioclase and pyroxene phenocrysts that show complex zoning (such as oscillatory or patchy zoning) and resorbed textures (dissolution surface or cellular zones). Coexistence of normally and reversely zoned pyroxene is common except the lavas from the early stage of Tangkil (three samples from Tkl 1) in which the orthopyroxene crystals are homogeneous and clear.

Lavas from Tangkil and Rajabasa Volcanoes are divided into three categories on the basis of the stage and petrographic characteristics: (a) Tangkil felsic rocks (Tklf), (b) Tangkil mafic rocks (Tklm), and (c) Rocks from Rajabasa (Rbs).

Tangkil felsic rocks (Tklf)

Tklf are porphyritic dacite containing phenocrysts of plagioclase, orthopyroxene, and Fe-Ti oxides (Figure 4a). These phenocryst minerals are embedded within a groundmass containing plagioclase, orthopyroxene, augite, apatite, and opaque minerals. Plagioclase in three samples from the early stage of Tangkil (26.02, I.6.03, 18.02) is clear, euhedral to subhedral, and smaller than 1.6 mm. Normal zoning and oscillatory zoning are developed. Hornblende phenocrysts occur in these samples. Orthopyroxene phenocrysts are euhedral to subhedral, and smaller than 1.3 mm. In the sample from the later stage (23.03; last Tklf) most plagioclase crystals are subhedral and the maximum crystal size is 2.4 mm. In this sample, plagioclase contains resorbed cores and cellular zones by An-rich clear rims. The cellular textures are developed either in the centres or margins of plagioclase crystals (Figure 4b). The cellular part comprises small inclusions of glass, pyroxene, and oxide minerals. Clinopyroxene phenocrysts occur together with orthopyroxene, and they are subhedral to anhedral with size of <0.8 mm. The clinopyroxene aggregates with plagioclase and orthopyroxene. Some discrete and clinopyroxene/orthopyroxene in the aggregates show both normal and reverse zoning.

Tangkil mafic rocks (Tklm)

Tklm (samples 24.02 and 24.03 from Tkl 2) are porphyritic basalt containing phenocrysts of plagioclase, Fe-Ti oxides, and olivine replaced by iddingsite (figure 4c). The groundmass comprises plagioclase, augite, pigeonite, opaque minerals, and glass. These rocks are highly porphyritic (33 - 37 vol. % phenocrysts). Phenocrysts occur mostly as discrete crystals, and glomerocrysts are not common. Plagioclase crystals are 0.1−2.5 mm in size, and show euhedral to subhedral shape. The most common euhedral plagioclase phenocrysts show normal zoning, consisting of clear cores. The reverse-zoned plagioclase is not found. Some subhedral plagioclase phenocrysts show rounding of edges (Figure 4c) and sieve textures. Plagioclase crystals without sieve textures are commonly smaller (< 1.8 mm) than plagioclase with sieve textures.

Rocks from Rajabasa (Rbs)

The samples from Rbs are composed of andesite, basaltic andesite, and basalt. They show porphyritic texture with the phenocryst abundance ranging from 38 to 51 vol. %. The phenocrysts are 0.2 to 4.3 mm in size. Phenocrysts of plagioclase, orthopyroxene, clinopyroxene, and Fe-Ti oxides are abundant in all samples. Additionally, some of the samples alternatively contain either a combination of biotite ± hornblende or olivine ± spinel as phenocrysts. Phenocryst minerals occur both as discrete crystals and glomeroporphyritic aggregates (Figure 4d). The aggregates comprise a combination of olivine, plagioclase, orthopyroxene, clinopyroxene, biotite, hornblende, and Fe-Ti

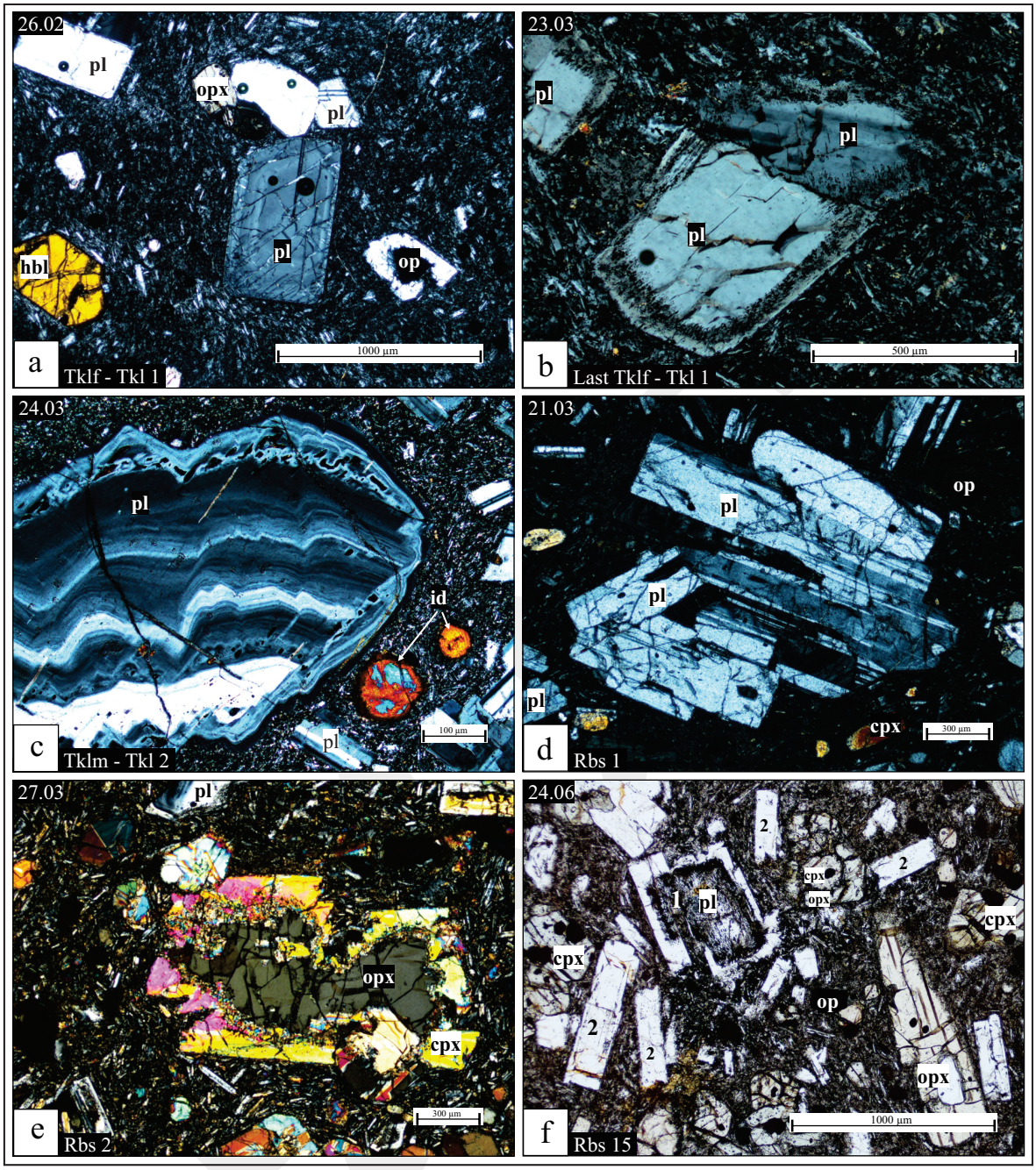

Figure 4. Representative cross polar photomicrographs of: a) Euhedral phenocrysts of plagioclase (pl), fresh amphibole (hbl), and pyroxene (opx); b) Subhedral plagioclase (pl) containing cellular zones in the margin of crystals; c) Plagioclase with complex zoning (pl) and iddingsite (id) with altered olivine; d) An aggregate of plagioclase phenocrysts (pl) and discrete augite crystals; e) Orthopyroxene (opx) mantled by clinopyroxene rim (cpx). Melt inclusions developed in resorption boundary between the two phases; f) Phenocrysst assemblages in Rbs, containing spongy cellular or sieved plagioclase crystals (type 1) and "clear" plagioclase crystals (type 2).

oxides. The most common aggregates comprise orthopyroxene, clinopyroxene, plagioclase, and opaque minerals. The groundmass comprises plagioclase, orthopyroxene, augite, apatite, opaque, and minor glass.

Orthopyroxene phenocrysts are commonly more abundant and bigger (<1.5 mm) than clinopyroxene (< 1 mm). The occurrence of orthopyroxene phenocrysts that are mantled by clinopyroxene (augite) rim (Figures 4e and 5f) is prevalent in the

olivine-rich basaltic andesite samples (Rbs 2 in Table 2). Both homogeneous and zoned pyroxene phenocrysts are present. The zoned pyroxene crystals show either normal or reverse chemical zoning in all lava units, except for Rbs 8 (Figures 5d, 5e). As shown in the back-scattered electron (BSE) images and line scan profiles of augite crystals in an andesite of Rbs 18 (Figure 6), some clinopyroxene crystals show reverse zoning with a low Mg/Fe core and a high Mg/Fe rim (spectrum 1), whereas other coexistent clinopyroxene crystals show normal zoning with a high Mg/Fe core and a low Mg/Fe rim (spectrum 2). It is also noted that spectrum 2 shows a slight increase of Mg/Fe in the most-rim part. The BSE image (Figure 5e) shows a step reverse zoning in augite of which the composition sharply changes from the iron-rich core (low Mg/Fe) to the magnesium-rich (high Mg/Fe) mantle. The Fe-rich cores are anhedral with rounded and embayed characteristics. By contrast, rounded and embayed cores do not occur in normally zoned clinopyroxene (Figure 5d). Olivine crystals vary in size, from 0.1 mm to 1.9 mm. Most olivine phenocrysts are subhedral to euhedral. The smaller, the more rounded the olivine crystals are. Olivine occurs as discrete crystals, and in some cases as

Table 2. Whole Rock Compositions of Rajabasa (Rbs) and Tangkil (Tkl)

Unit	**Rbs 1**				**Rbs 2**		**Rbs 6**		**Rbs 7**	**Rbs 8**	**Rbs 9**	**Rbs 10**	
Sample	**26.05a**	**26.05b**	**21.03**	**I.22.04**	**27.03**	**I.7.10**	**I.9.04**	**I.15.01**	**25.03**	**I.8.01**	**I.2.04**	**I.22.02**	**I.8.08**
Major elements (wt %)													
SiO_2	59.86	59.30	60.89	61.30	54.54	54.09	59.12	59.43	59.81	51.06	58.39	57.86	60.34
TiO_2	0.84	0.85	0.81	0.74	0.85	0.80	0.87	0.72	0.83	1.10	0.82	0.96	0.82
Al_2O_3	17.65	17.38	16.81	17.02	16.68	16.82	17.66	17.27	17.21	18.86	17.89	17.56	17.27
FeO*	6.18	6.90	7.23	6.26	7.12	7.56	7.03	6.58	6.96	9.12	7.38	7.84	6.70
MnO	0.12	0.14	0.15	0.13	0.20	0.15	0.15	0.14	0.14	0.18	0.15	0.15	0.14
MgO	2.90	3.08	2.65	2.90	6.12	7.11	3.01	3.39	2.68	5.94	3.09	3.21	2.88
CaO	6.36	6.39	5.50	5.80	10.03	9.14	6.27	6.80	6.06	9.14	6.68	6.78	5.95
Na_2O	3.63	3.59	3.37	3.27	2.85	2.79	3.42	3.28	3.81	3.15	3.43	3.53	3.23
K_2O	2.25	2.16	2.40	2.40	1.40	1.34	2.21	2.22	2.19	1.12	1.92	1.85	2.45
P_2O_5	0.22	0.21	0.20	0.18	0.19	0.19	0.26	0.17	0.30	0.35	0.24	0.24	0.22
L.O.I.	0.55	0.88	1.65	1.42	0	0.23	0.98	0.93	0.43	1.48	0.91	0.56	1.41
H_2O (-)	0.29	0.35	0.71	0.28	0	0.04	0.15	0.18	0.27	0.17	0.12	0.22	0.19
Trace elements (ppm)													
Rb	71	66	79	82	42	40	67	75	68	24	66	55	75
Ba	387	368	432	451	258	283	397	372	401	298	383	319	347
Sr	479	473	416	397	448	412	431	411	493	592	489	470	426
Zr	140	135	138	149	100	100	151	129	160	114	128	133	147
Nb	5	4	5	23	5	19	22	24	7	28	26	14	30
Y	24	22	27	29	36	22	25	23	34	26	27	27	31
Cr	11	13	11	14	250	245	10	30	13	37	7	6	6
Ni	10	10	8	5	114	96	4	13	10	21	2	3	3
V	170	171	164	154	217	210	182	174	146	227	164	206	168

The data is normalized to 100% with volatile-free basis.
*Total iron as FeO

Table 2. continued...

Unit	Rbs 11	Rbs 15	Rbs 16		Rbs 18					Tkl 2 / Tklm		last Tklf	Tkl 1 / Tklf		
Sample	**I.21.06**	**24,06**	**I.14.03**	**I.20.08**	**19.02a (xenolith)**	**19.02b**	**I.10.03**	**23,02**	**20,02**	**24,02**	**24,03**	**23,03**	**26,02**	**I.6.03**	**18,02**
Major elements (wt %)															
SiO_2	61,67	56,18	55,78	56,42	53,35	61,05	58,70	58,27	60,93	51,41	52,28	66,52	69,03	69,01	70,88
TiO_2	0,70	0,89	0,94	0,85	1,16	0,78	0,74	0,78	0,76	1,15	1,29	0,54	0,70	0,65	0,56
Al_2O_3	16,93	17,96	18,41	18,14	18,48	16,41	17,67	17,07	16,70	20,06	19,86	15,88	16,11	16,12	16,00
FeO*	6,11	8,09	7,97	8,03	8,46	6,39	6,76	7,00	6,27	9,39	9,41	4,02	3,20	3,27	2,58
MnO	0,14	0,16	0,16	0,16	0,15	0,14	0,14	0,15	0,14	0,16	0,15	0,09	0,09	0,11	0,03
MgO	2,75	3,87	3,74	3,96	4,14	2,89	3,65	4,07	2,83	3,52	2,89	1,83	0,51	0,65	0,14
CaO	5,87	7,57	7,91	7,37	9,56	6,18	6,83	7,03	6,31	10,39	9,78	4,17	2,59	2,63	1,48
Na_2O	3,13	3,48	3,15	3,31	3,27	3,55	3,20	3,36	3,50	3,08	3,28	4,13	4,57	4,51	5,35
K_2O	2,52	1,59	1,74	1,54	1,24	2,44	2,16	2,11	2,41	0,61	0,80	2,72	3,04	2,88	2,93
P_2O_5	0,18	0,22	0,20	0,23	0,18	0,16	0,16	0,16	0,15	0,23	0,26	0,11	0,16	0,17	0,05
L.O.I.	1,08	0,68	0,80	0,64	0,09	0,66	0,77	0,39	0,56	0,78	1,13	1,55	3,04	2,88	2,22
H_2O-	0,14	0,28	0,10	0,15	0,20	0,18	0,13	0,30	0,15	0,31	0,46	0,66	0,42	0,23	1,10
Trace elements (ppm)															
Rb	81	44	54	46	23	80	72	68	80	12	24	88	77	74	78
Ba	427	299	287	265	232	422	338	355	397	160	191	386	421	394	493
Sr	411	508	474	474	596	415	409	438	421	489	476	249	244	237	203
Zr	141	117	114	116	83	126	129	128	125	102	127	190	313	310	286
Nb	23	3	23	28	3	4	21	4	3	4	4	5	11	36	8
Y	62	22	27	22	22	22	21	22	21	26	29	23	46	45	30
Cr	9	19	13	14	23	11	32	39	13	41	31	30	10	0	6
Ni	4	14	4	10	10	10	10	18	9	15	10	23	11	5	11
V	157	235	227	211	305	161	185	186	199	262	284	99	39	12	12

The data is normalized to 100% with volatile-free basis.
*Total iron as FeO

aggregates with clinopyroxene and plagioclase. Spinel often appears as inclusions in big olivine and rarely in pyroxene and plagioclase. Fe-Ti oxide minerals occur as abundant titanomagnetite and rare ilmenite.

Except for lava from Rbs 8, all unit lavas contain two distinct types of plagioclase crystals; type 1 is characterized by the presence of complex zoning and resorption textures, whereas type 2 is characterized by clear crystal (Figure 4f). The type 1 occurs as subhedral crystals bigger than 0.4 mm. Resorption textures are common, shown by unconformable or irregular surfaces between Ca-poor core and Ca-rich mantle (Figure 5a) and by spongy cellular zones (Figure 5c). The anhedral cores are surrounded by a Ca-rich mantle (Figure 5a). In addition to the resorbed core, the patchy-zoned cores and clear cores are also common. Coarsely spongy cellular zones showing resorption channels which typically occupy the entire crystal from core to rim, whereas finely spongy cellular zones (also termed as "sieved") are overgrown by a clear and zoned rim with the thickness of up to 0.1 mm. Melt inclusions in the resorption channels or sieved zone commonly include glass, pyroxene, and oxide minerals. In some crystals,

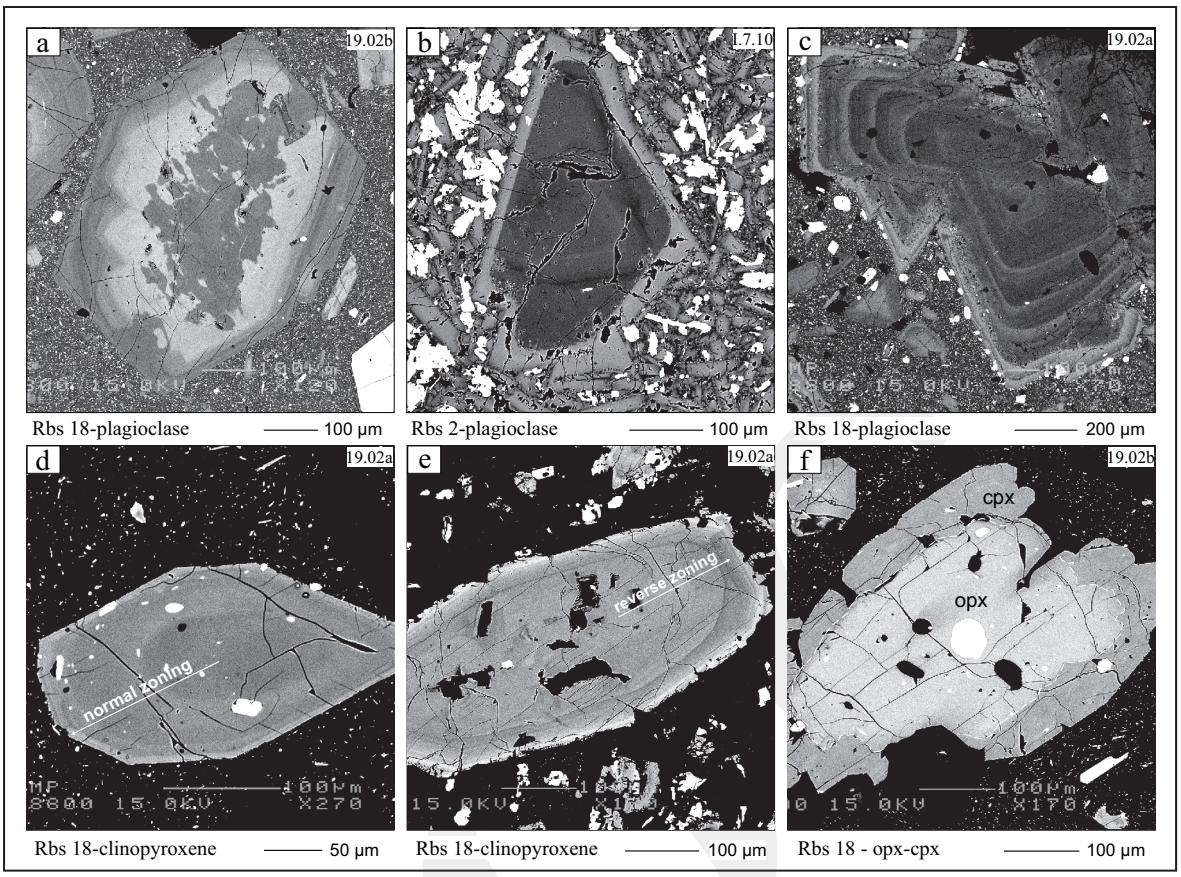

Figure 5. Back-scattered electron images of phenocrysts showing textures and compositional differences. a) Resorbed core with calcic-rich mantle (light shade) in plagioclase. b) The inner growth bands are dissected by calcic-rich plagioclase. c) Oscillatory (multiple) zoned plagioclase with transition between growth bands bound by calcic-rich and dissolution surfaces. Sieved zoned near the rim contains melt inclusions. d) Progressive normal zoning in clinopyroxene. e) Reverse step zoning in clinopyroxene. The transition is marked by abrupt increase in Mg# (rounded dark layer) in mantle. Core is embayed and slightly patchy. f) Orthopyroxene (opx) mantled by clinopyroxene (cpx) rim. Darker shade in clinopyroxene reflect higher Mg#.

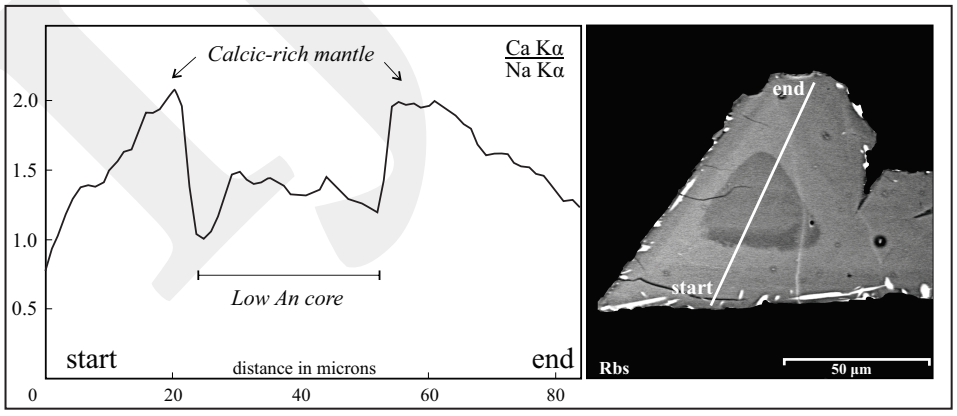

Figure 6. Step reverse zoning shown by plagioclase phenocryst from Rbs samples. Anhedral calcic-poor core (dark shade) mantled by calcic-rich (light shade) plagioclase.

patchy texture is exhibited in sieved region. Complex oscillatory zoning shows multiple growth zones that are separated by high Ca/Na bands (Figure 5c). From core, the Ca/Na decreases outward, abruptly increases, and gradually decreases again toward the next growth band. The anhedral inner part is dissected by a sharp boundary, dissecting the growth bands discordantly. The multiple

growth zones do not develop in other minerals. On the other hand, type 2 is commonly euhedral and occurs in various size. Clear plagioclase phenocrysts show normal, reverse, or oscillatory zoning. Reversely, zoned plagioclase contains a subhedral Ca-poor core that is overgrown by a Ca-rich mantle (Figure 6). Type 1 and type 2 plagioclase coexist in individual aggregates, in which the latter type is more abundant.

Major and Trace Element Variations

The studied samples of this volcanic area exhibit a large variation in SiO_2 (51-71 wt %) (Figure 7). The compositional ranges of Na_2O, K_2O, and MgO are 2.8-5.4 wt %, 0.6-3.0 wt %, and 0.1-7.1 wt %, respectively (Table 2). The variations of MgO and SiO_2 are roughly correlated with the mafic phenocryst assemblages (Figure 7). Phenocryst assemblages of high-SiO_2 and low-MgO lavas from the Tkl 1 is pl + opx + opq ± cpx ± hbl. On the other hand, the low-SiO_2 lavas from the Tkl 2 are pl + ol + opq. The least magnesian samples from Rajabasa (Rbs 1 and Rbs 11 in Table 2) contain phenocryst of pl + opx + cpx + opq + bt + hbl, and the phenocryst assemblage of the most magnesian samples (Rbs 2 and Rbs 8) is pl + opx + cpx + opq + ol ± spl. Spinel occurs in Rbs 2, Rb 6, and Rbs 18. Only andesitic samples with SiO_2 above *c.* 60 wt % contain biotite and hornblende. The occurrence of olivine in Rajabasa is not correlated with the whole rock composition as olivine is lacking in some andesite samples (Rbs 1, 7, 9, and 11), but present in more evolved samples (Rbs 10 and Rbs 18) with biotite and hornblende. Olivine crystals in samples with SiO_2 <56 wt % and MgO ≥6 wt % (Rbs 2 and Rbs 8) are up to 1.9 mm in size and abundant, whereas the olivine in samples with SiO_2 >56 wt % is < 0.7 mm in size and sporadic. Basaltic andesite from Rbs 2 is higher in MgO than that of basalt from Rbs 8. Compared to the less magnesian samples, the high MgO samples have more clinopyroxene than orthopyroxene.

Volcanic rocks from Tangkil are classified as medium-K basalt (51-52 wt % SiO_2; Tklm) and medium- to high-K dacite to rhyolite (67-71 wt % SiO_2; Tklf), whereas those from Rajabasa are basalt, basaltic andesite, and andesite (51−62 wt % SiO_2; Rbs) (Figures 8 and 9). The high-SiO_2 samples of Rbs are classified as high-K andesite, whereas the low-SiO_2 lavas are either medium-K basalt or basaltic andesite. Tklf and Tklm show discontinuous, separated iron-enrichment trends on the modified Miyashiro diagram (FeO^t/

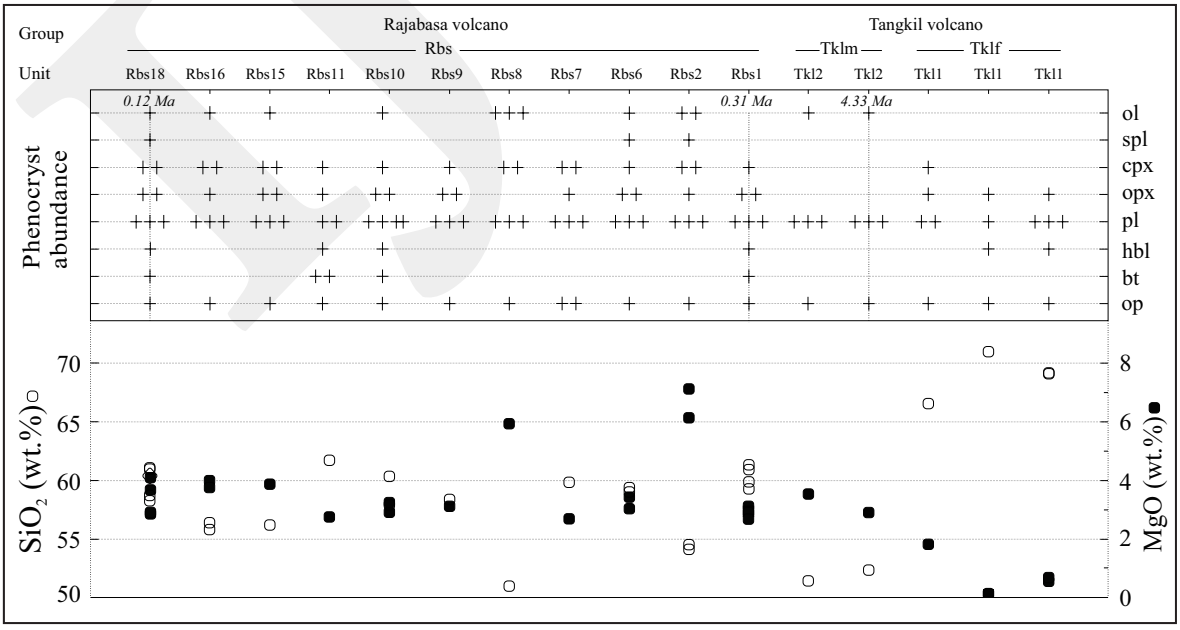

Figure 7. Phenocryst abundance variations in samples from Tangkil and Rajabasa Volcanoes. Modal abundance of 0−5%, 5-10%, and 10-30% are indicated by symbol +, ++, and +++, respectively.

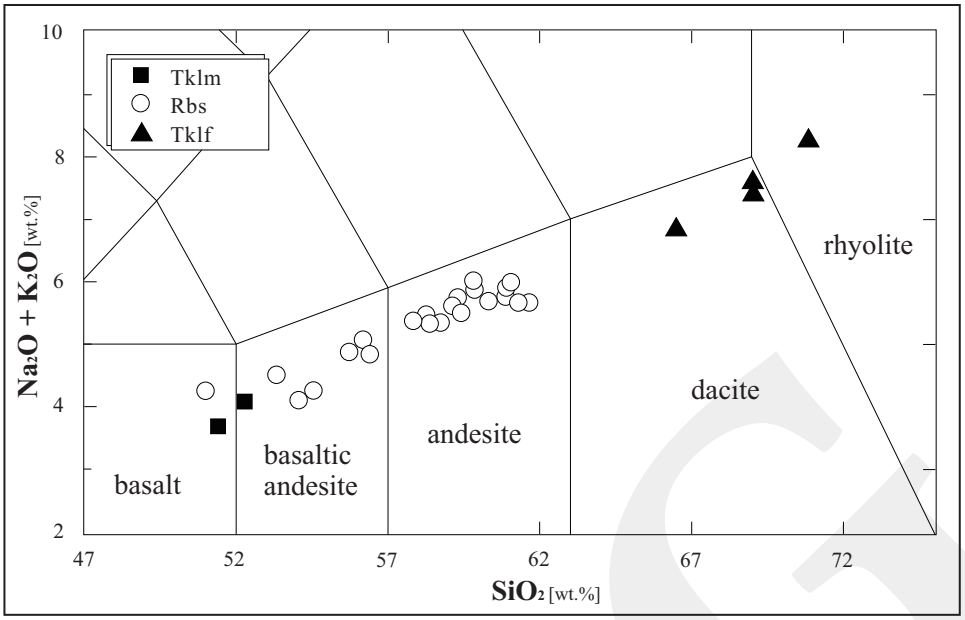

Figure 8. Rock classification using the scheme of Le Bas *et al*. (1986) based on the total alkali ($Na_2O + K_2O$ wt %) *vs* silica (SiO_2 wt %) diagram for Tangkil and Rajabasa volcanic rocks. Except for Rbs 8, the majority of the rocks from Rajabasa plot in the basaltic andesite to andesite fields (circle), whereas rocks from Tangkil plot in two cluster ends (rectangle and triangle).

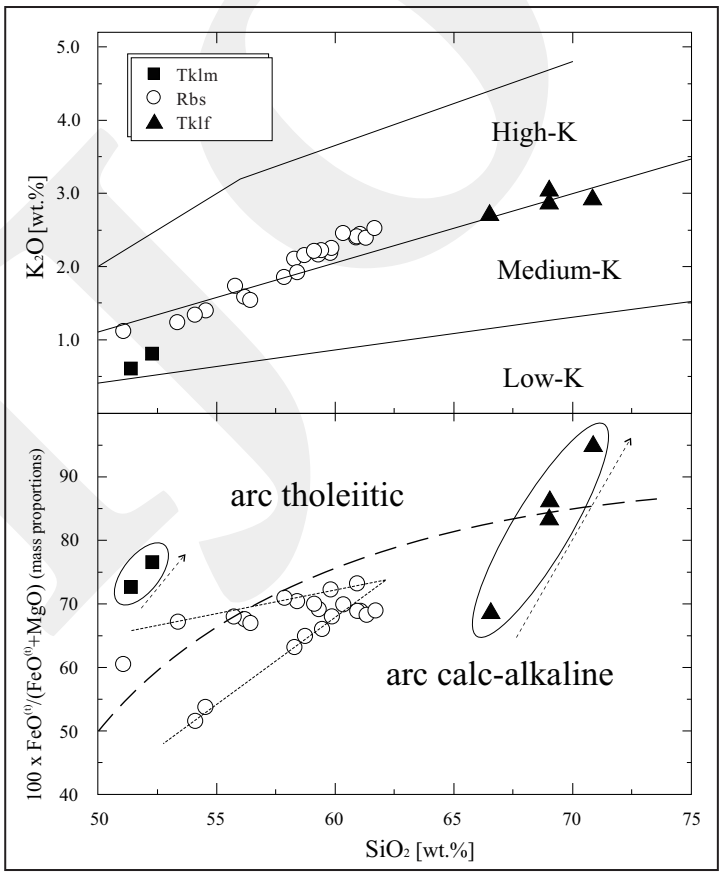

Figure 9. Diagram of silica *vs* K_2O for the subdivision of the subalkaline series (Le Maitre *et al*., 1989). Rbs and Tklf rocks are plotted in transition from medium-K to high-K, whereas Tklm rocks plotted in medium-K (above). A discriminating diagram between tholeiitic and calc-alkaline magma series. The separating line (heavy dashed line) is from Miyashiro (1974) which was later modified by Gill (2010) (below).

(FeO^t+MgO) *vs* SiO_2) (Figure 9) (Miyashiro, 1974; Gill, 2010). The extrapolations of the trends do not cross as they are subparallel. The two samples from Tklm show an iron-enrichment which is typical of tholeiitic basalt. Tklf displays an iron-enrichment trend parallel to the basalt trend and crosses the boundary between calc-alkaline and tholeiitic fields. Rbs show two different trends; one is near-constant $FeO^t/(FeO^t+MgO)$, and the other is a steep iron-enrichment trend. Two samples that are the mafic end of the steep iron-enrichment trend are olivine-rich basaltic andesite samples (Rbs 2). The high-silica samples of Rbs cluster at an andesite composition, at which the two trends converge.

Variation diagrams of selected major and minor elements *vs*. SiO_2 are shown in Figure 10. Rocks from Tklf show clear negative correlation of SiO_2 with $FeO^{(t)}$, MgO, CaO, and Sr and positive correlation with alkali and Ba. The last Tklf sample show the lowest TiO_2 content in the series. On the diagrams of TiO_2, MgO, Al_2O_3 *vs* SiO_2, Tklf trend is not continuous with Tklm trend. Rocks from Tklm show a positive silica correlation with TiO_2 and negative silica correlation with MgO, CaO, and Al_2O_3. Tklm samples are lower in MgO than the basalt samples of Rajabasa. Rocks from Rajabasa show positive correlations in alkali, Rb, Ba, and Zr but negative correlations in TiO_2, $FeO^{(t)}$, MgO, CaO, Al_2O_3, and Sr against silica. The silica-variation plots of MgO, Al_2O_3, and Sr show two different trends which converge at *c.* 62 wt % SiO_2. Two olivine-rich basaltic andesites (Rbs 2) plot at the high-MgO end of the trend on MgO vs. SiO_2 diagram. In addition, they plot off lower the other trend of TiO_2, $FeO^{(t)}$, Al_2O_3, and Sr. Except for these basaltic andesite samples, Ni and Cr are as low as 8 - 23 ppm and 6-41 ppm, respectively. These two samples are extraordinarily high in Ni (95 - 114 ppm) and Cr (*c.* 250 ppm), which are higher than those of basalt samples from Rbs and Tklm. The contents of Ni and Cr from the last Tklf sample (67 wt. % SiO_2) are the highest in the series. Furthermore, the content of Ni is slightly higher than samples of Tklm and Rbs except for the two high-MgO samples from Rbs 2. On the diagrams of K_2O *vs* MgO and Rb *vs* Cr, two linear trends of Rbs converge at *c.* 2.7 wt % K_2O at the lowest MgO of 2.2 wt % and at *c.* 83 ppm Rb at the lowest Cr of 5 ppm (Figure 11).

The temporal chemical variation of Tangkil and Rajabasa is shown in Figure 12. The equivocal order of two flow units is depicted in temporal chemical variations with the parallel ages (Rbs 1 - Rbs 2; Rbs 7 - Rbs 8; Rbs 9 - Rbs 10). Before *c.* 4.3 Ma, Tangkil Volcano was initiated by the eruption of dacite and rhyolite lavas (Tklf). In this period, SiO_2 and Na_2O+K_2O initially increased, and then decreased. The opposite trends are apparent in CaO and MgO. In *c.* 4.3 Ma, Tangkil Volcano changed its eruption products from dacite/rhyolite to basalt (Tklm). The two samples from Tklm show a slight increase in CaO and MgO and a decrease in SiO_2 and Na_2O+K_2O. The Al_2O_3 contents from Tklf and Tklm do not change through time, 16 wt. % and 20 wt. %, respectively. Then at *c.* 0.31 Ma, Rajabasa Volcano started its activity by erupting basaltic andesite and andesite of which SiO_2 fluctuates from 54 wt. % to 62 wt. %. The majority of Rbs shows rising-falling variation in SiO_2 and MgO. The concentrations of Na_2O+K_2O comply with SiO_2, whereas those of CaO, MgO, and Al_2O_3 are the contrary. Basaltic andesite and basalt are marked with spikes of CaO (9.1 - 10 wt %) and MgO (5.9 - 7.1 wt %), while differentiated andesite are produced constantly. The lavas with high-Mg basaltic andesite and basalt composition (Rbs 2 and Rbs 8) are olivine-rich rocks and originated from the older Balerang cone. These Mg-rich rocks are intercalated with the differentiated andesite.

Discussion

The Volcanism of Tangkil and Rajabasa

This study elucidated the history of volcanism in Tangkil and Rajabasa Volcanoes. The volcanism was commenced by the eruption of Tangkil Volcano. The early activity of Tangkil is characterized by felsic magma (Tklf), whereas

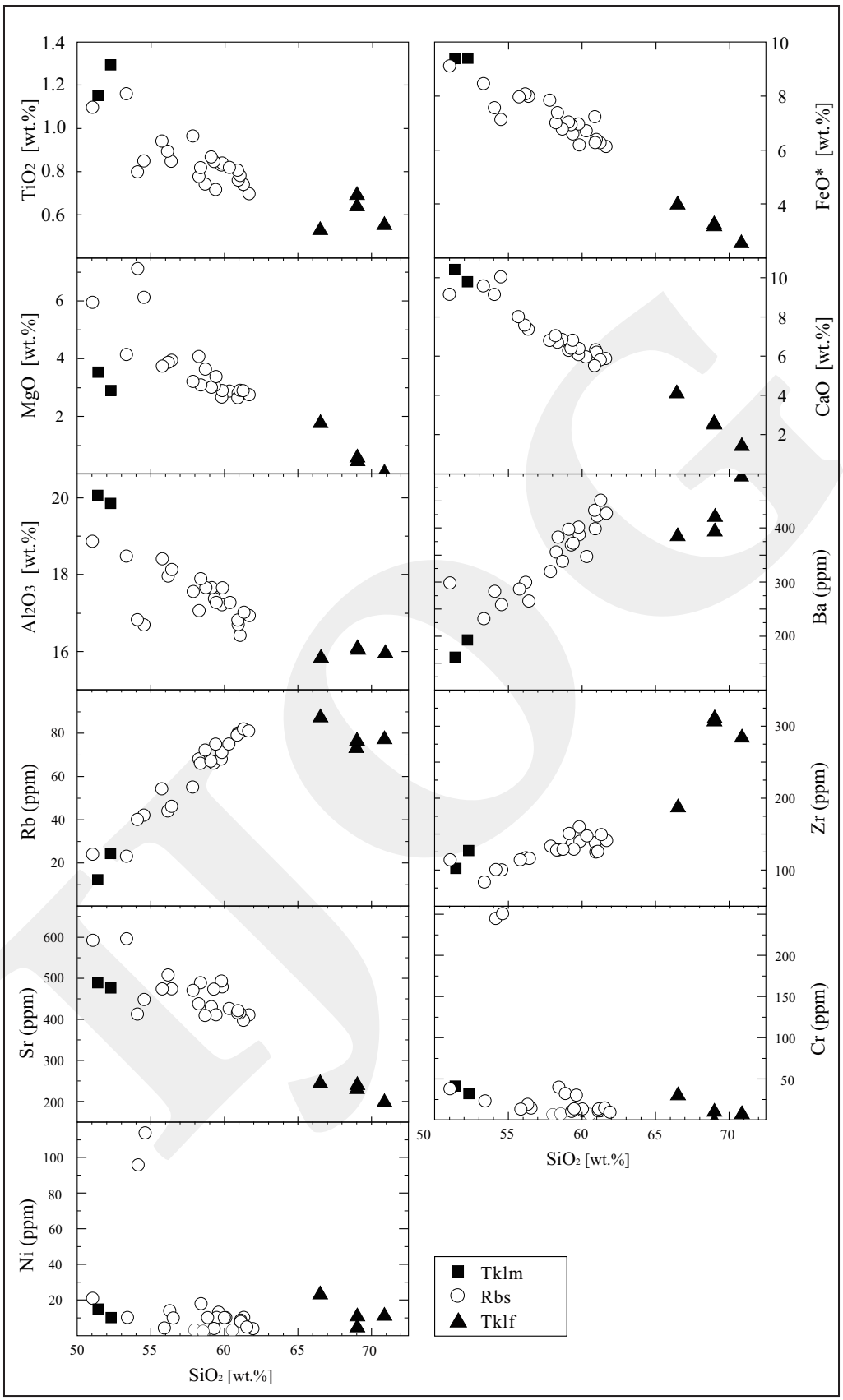

Figure 10. Variation diagrams of SiO_2 (wt.%) *vs*. selected major and minor elements (ppm) for Tangkil and Rajabasa volcanic rocks.

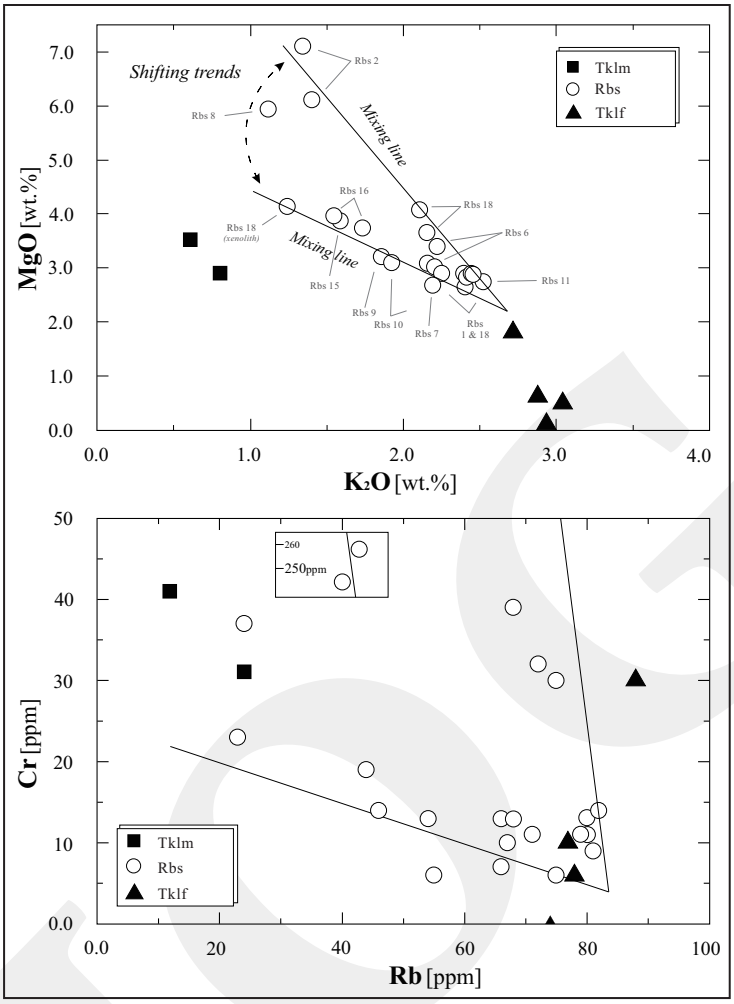

Figure 11. Tangkil and Rajabasa volcanic rocks plotted in K_2O *vs* MgO and Rb *vs* Cr. The diagrams display two discontinuous trends from Tangkil Volcano, which are not parallel with Rajabasa trends. Meanwhile, Rajabasa Volcano depicts two trends that converge from high-Mg and low-Mg basaltic composition to andesitic composition.

the later activity in *c.* 4.3 Ma is characterized by mafic magma (Tklm). Then, the volcanic activity was halted. After termination of the activity of Tangkil Volcano, it took *c.* 4 Ma to resume the volcanic activity at Rajabasa Volcano. The ages of commencement and cessation of Rajabasa volcanism are in *c.* 0.3 Ma and *c.* 0.1 Ma, respectively. The activity of Rajabasa is characterized by the presence of major intermediate and minor mafic lavas. The most mafic samples (olivine-rich basaltic andesites of Rbs 2 and basalts of Rbs 8) are produced by the older eruption centre of the Balerang cone (Figure 9).

The volcanism in the area is likely to be affected by the tectonic setting. The clockwise rotation of Sumatra relative to Java which preceded the activity of Rajabasa has started since at least 2.0 Ma (Ninkovich, 1976; Nishimura *et al*., 1986). The changes of the volcanic centre from Tangkil to Rajabasa and the eruption centre from the Balerang cone to the Rajabasa cone is parallel with the major NW−SE fault zone in Sumatra (Sumatra Fault System). This crustal scale strike-slip faulting may have provided different paths for the magma to rise. A similar idea has been suggested by Bronto *et al.* (2012) who presumed that the change of eruption centre in Rajabasa Volcano was controlled by a deep fracture. A number of studies have also proposed a similar influence of strike-slip faulting on volcanism (*e.g.* Fytikas and Vougioukalalis, 1993; Piper and Perissoratis, 2003; Pe-Piper *et al*., 2005).

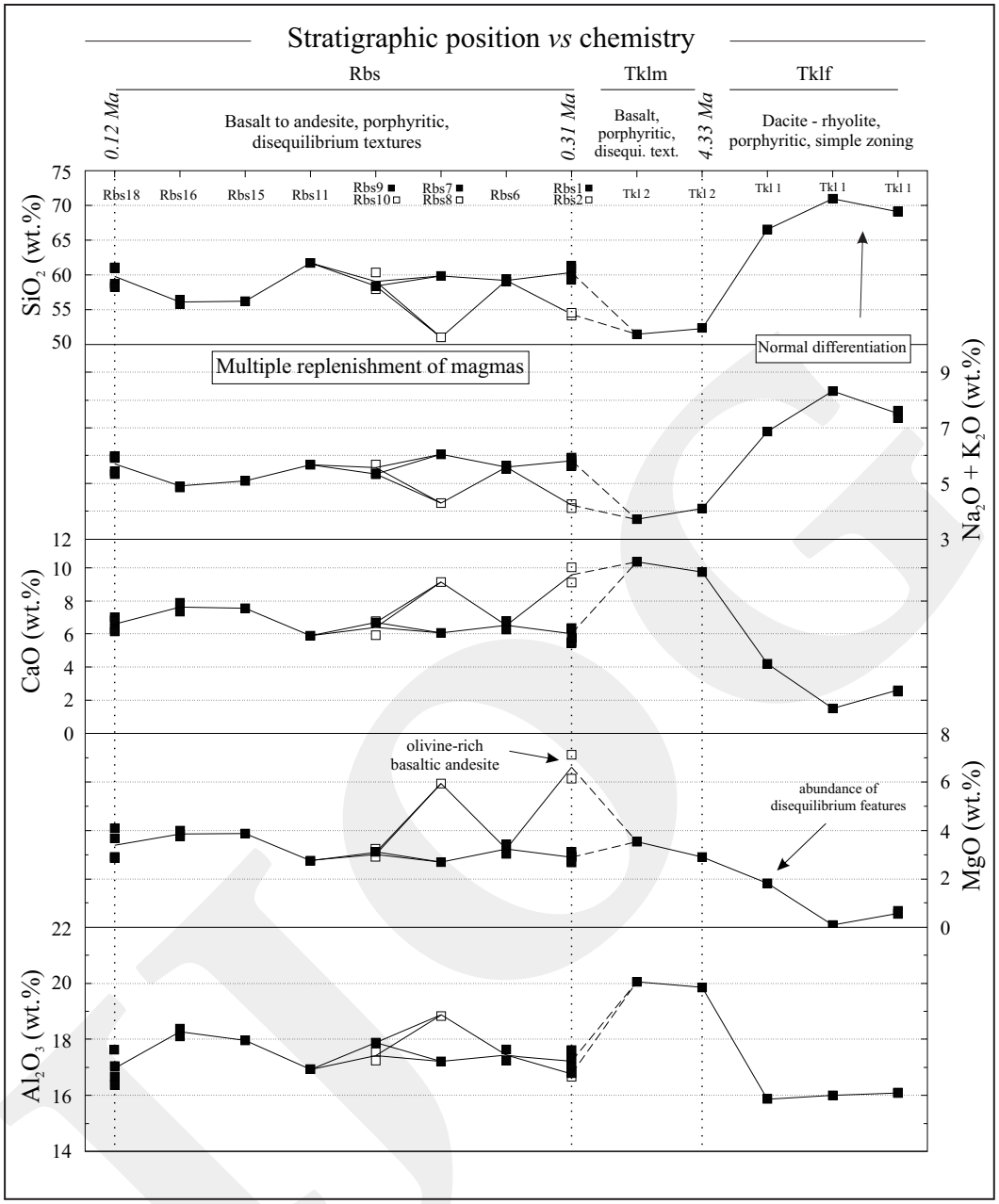

Figure 12. Temporal chemical variation of Tangkil and Rajabasa volcanic rocks. Total alkali (Na_2O+K_2O) composition trend complies with silica (SiO_2), whereas CaO, MgO, and Al_2O_3 do not follow silica composition trend. All samples composition for each unit are plotted; continuous lines are running average from all sample in each unit to show the trend of the data.

Open System Magmatic Process

The open system magmatic processes are indicated by petrographic evidence for the rocks from the last Tklf and Rbs. This evidence includes resorbed textures in plagioclase, such as dissected zoning, irregular and patchy core, as well as cellular or sieved texture with melt inclusions (Figures 4b, f, and 5a - c). The resorbed textures in plagioclase reflect changes in magmatic condition experienced during the crystal growth (*e.g.* Humphreys *et al*., 2006). Partial dissolution of plagioclase can be caused by heating, hydration of melt, decompression, or a combination of these processes (*e.g.* Tsuchiyama, 1985; Nakamura and Shimakita, 1998; Nelson and Montana, 1992). Once in a reservoir, the differentiation of magma continued in cooling, convection, decompression, and recharge of new magmas. Partial

dissolution of crystal exterior is characterized by the overgrowth of Ca-rich plagioclase on the crystal surface (Figures 5b and 6). This texture is consistent with the experimental results of Nakamura and Shimakita (1998), who invoked the dissolution-recrystallization origin. Anorthite zonation represents the history of ambient magmatic conditions as diffusion rate of NaSi-CaAl is low relative to timescales of magmatic event. The irregular or sieved cores/mantles and clear euhedral rims are formed under different conditions and stages. Dissolution textures were formed by one or combination processes of heating, hydration, or decompression. Then, the recrystallization of higher Ca/Na mantle/rim progressed after the dissolution process

The resorption-overgrowth texture in pyroxene crystals also represents the open system processes. Anhedral and rounded cores in pyroxene suggest the resorption process (Figure 5e). The resorbed cores are only developed in reversely zoned clinopyroxene. The Fe-rich cores are characterized by embayed morphology and unconformable interfaces with mantle, indicating resorption of Fe-rich pyroxene. The dissolution surface in pyroxene develops in response to an external factor such as the temperature increase above their liquidus, compositional change (including oxygen fugacity), or decompression. The resorbed core is overgrown by a less evolved (higher Mg/Fe) mantle or rim, implying resorption-overgrowth was induced by a change in ambient magma composition from low Mg/Fe to high Mg/Fe (mafic) composition. The Mg-rich mantle shows normal zoning with polygonal growth bands (Figures 5d and e), indicating progressively evolving composition of melt during cooling. The coexistence of augite-mantled orthopyroxene with clear euhedral orthopyroxene, as well as normal and reverse zoning of clinopyroxene in the same sample reflects the wide variation (Figure 5f). The texture of orthopyroxene mantled by augite can be explained by heating and compositional change of melt (*e.g*. Gerlach and Grove, 1982), where the orthopyroxene was resorbed first, overgrown then by augite.

Of the two types of plagioclase and pyroxene, resorption of evolved core and overgrowth of less evolved mantle can be accounted by a temperature rise, influx of volatile (to reduce T of liquidus and to change equilibrium composition), or change of chemical composition of ambient magma to higher MgO/FeO and higher CaO/Na_2O. The multiple zones of dissolution-overgrowth textures in plagioclase crystals (*i.e.* Figure 5c) indicate that the changes of magmatic condition in T, H_2O, or chemical composition were repetitive. The lack of multiple dissolution-overgrowth layers in other minerals implies faster chemical diffusion rate than that in plagioclase (Grove *et al*., 1984; Morse, 1984).

Magma mixing is indicated by the whole-rock chemistry diagrams (*e.g*. Figures 10 and 11). Fractional crystallization trends are concave-upward in diagrams of MgO *vs* SiO_2. Two linear trends on the diagram (Figure 11), except for a transitional endmember of Rbs 8, indicate the mixing of two mafic endmembers with a felsic endmember. MELTS software (Ghiorso and Sack, 1995; Gualda *et al*., 2012) was used to evaluate and model the fractional crystallization trends. The composition of 50 wt % SiO_2 for both mafic endmembers was assumed and other elements was determined by extrapolating the trend of the elements to the assumed SiO_2 content; the total obtained for both was 100 wt %. The system was assumed did not contain free-water at liquidus, then by trial-and-error calculations the water content of 2 wt % was determined and fugacity constrained to QFM buffer. The calculation of phase relations under these conditions could produce the phenocryst assemblage of ol+sp+cpx+opx+pl. Three individual isobaric calculations (at 1, 2, and 3 kbar) show that no model result of fractional crystallization resembles the data for each mafic endmember trend, although at lower pressure (1 kbar) the simulated curves approximate the observed trends (Figure 13). In Figure 12, the spikes of CaO and MgO indicate that the recharges of high-Mg mafic endmember are sporadic, whereas the recharges of low-Mg mafic endmember are common during the entire lifetime of Rajabasa.

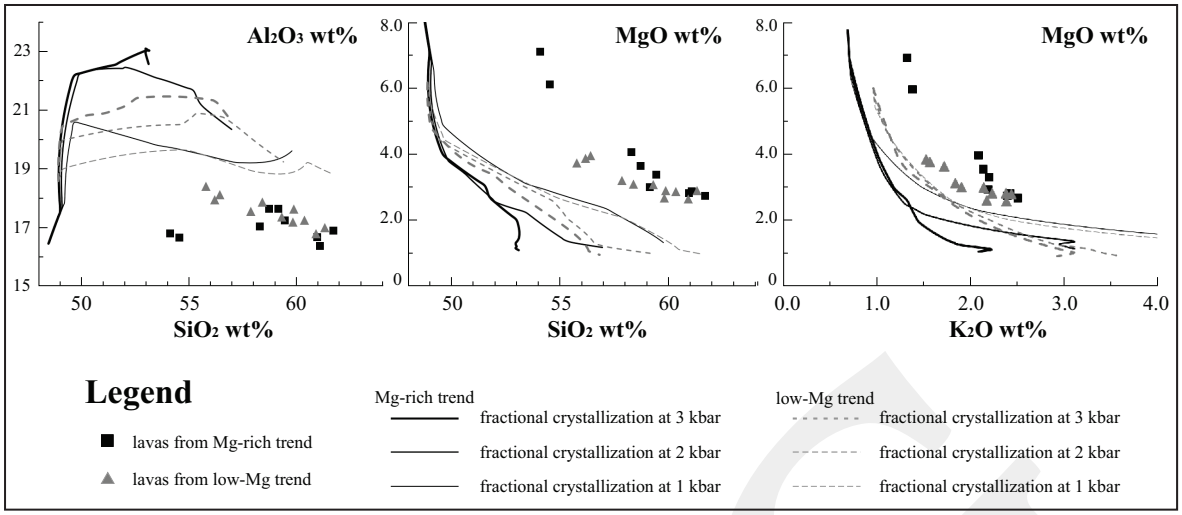

Figure 13. Modeling of major elements fractional crystallization with MELTS presented on Harker diagrams for Rajabasa. The parameters used in calculation are described in the text. Lines of fractional crystallization with pressures of 1, 2, and 3 kbar are shown. Samples of 19.02a and I.8.01 were excluded from calculation.

The last Tklf also underwent recharge of mafic magma, indicated by the whole-rock compositional variation of low-SiO_2, high-MgO, -Ni, and -Cr (Figure 12), and by the mineral textures of plagioclase and pyroxenes shown above.

The evidence of repetitive magma recharges is also represented by the fluctuating temporal whole-rock chemical variation which shows that differentiated andesite is intercalated with Mg-rich rocks (Figure 12). This variation can be produced by multiple replenishment of the evolved magma reservoir with mafic magma. Belkin *et al*. (1993), Villemant *et al*. (1993), and Gertisser and Keller (2003) found the similar variation and suggested multiple replenishments into a pre-existing magma reservoir. Based on the petrographical and geochemical evidences, it is concluded repeating magma recharges during the magmatic evolution of Rajabasa.

For the magma system at Rajabasa, at least three endmember magmas are identified: (1) Mg-rich medium-K basalt magma; (2) low-Mg medium-K basalt magma; and (3) high-K andesite magma (Figures 9 and 11). The high-Mg, medium-K basalt magma is a primitive magma with high Cr (>250 ppm) and Ni (>114 ppm) contents. Another basalt magma (2) is more differentiated, indicated by lower MgO, Cr, and Ni contents. The composition of the felsic endmember of Rajabasa Volcano is determined by the intersection of the two linear trends at an andesitic composition of ~2.2 wt % MgO and ~62 wt % SiO_2 (Figure 11). As discussed above, the Mg-rich medium-K basalt magma and the low-Mg medium-K basalt magma repeatedly injected into the high-K andesite magma.

Tangkil involves bimodal magma system of basalt and felsic magma. The felsic endmember of Tklf is more evolved, > 71 wt % SiO_2 and < 0.1 wt % MgO, than the felsic endmember of Rajabasa (Figure 11). The last Tklf could be a product of mixing between the felsic endmember and a mafic endmember.

The mineral assemblages in Rbs reflect the features of endmember magmas (Figure 7). The abundance of olivine in the silica-poor rocks implies that the olivine is originated from the mafic endmember. The presence of spinel-bearing rocks in MgO-rich trend indicates that spinel is derived from the Mg-rich medium-K basalt magma. Biotite and hornblende are originally crystallized from felsic endmember since they are abundant in the silica-rich rocks (SiO_2 > 60 wt %). The felsic endmember-derived minerals changed temporally and seem to be affected by temperature conditions in the felsic endmember reservoir. The felsic endmember magma stayed fixed in composition (at *c*. 62 wt % SiO_2), but its

temperature can change the mineral assemblage. Biotite and hornblende crystallize in a relatively low-T andesitic magma. Biotite and hornblende crystallized when the reservoir was cool, while they were not present when the reservoir was heated by mafic injections or the temperature was still high (like in early period). From the above discussion, cooling and heating of felsic magma reservoirs are repeated, resulted from the repeated injection or recharge of high-T mafic magma.

Conclusion

The volcanostratigraphic result combined with age dating analysis reveals that the volcanism in Tangkil commenced in *c.* 4.3 Ma and was characterized by dacite to rhyolite (Tklf) and basalt to basaltic andesite (Tklm) rocks; the commencement and cessation of Rajabasa volcanism were in *c.* 0.3 Ma and *c.* 0.1 Ma, respectively and characterized by basalt to andesite lavas (Rbs).

The plagioclase and pyroxene phenocrysts from the last Tklf and Rbs show resorption-overgrowth texture, a feature that can be caused by temperature rise, volatile influx, or compositional change of ambient magma. The repetitive changes of magmatic condition are indicated by the multiple zones of dissolution-overgrowth textures in plagioclase phenocryst as well as the fluctuating trend in the temporal whole-rock variation.

In the Rbs magma system, at least three different endmember magmas were involved: Mg-rich medium-K basalt magma; low-Mg medium-K basalt magma; and high-K andesite magma. The rising-falling variations in SiO_2 and MgO during the long evolution of magma indicate the three endmember magmas were active. The mixing of magmas is indicated by the whole-rock chemistry diagrams, petrography, and MELTS. The felsic endmember composition of Rajabasa is ~62 wt % SiO_2 and ~2.2 wt % MgO; Tangkil is > 71 wt % SiO_2 and < 0.1 wt % MgO.

The mineral assemblages in Rbs reflect the features of the three endmember magmas. The repeated injections of the Mg-rich medium-K basalt and the low-Mg medium-K basalt into the high-K andesite magma changed the temperature conditions in the felsic endmember reservoir that can affect the mineral assemblage of biotite and hornblende.

This study shows that the evolution of magma system and processes are reflected in the temporal petrological variations. But why the magmas mixed together during the activity of Rajabasa whereas they did not in Tangkil, remains an open question.

Acknowledgments

The authors sincerely appreciate CVGHM (Centre for Volcanological and Hazard Mitigation) in South Lampung and the people from Cugung Village who helped the authors during field observation. The authors also acknowledge Prof. Benyamin Sapiie at the Bandung Institute of Technology for the provision of satellite imagery of Rajabasa Volcano. This work is part of PhD. thesis by the first author at Akita University and was supported by Japan Society for the Promotion of Science (JSPS) leading programme "New Frontier Leader Program for Rare-metals and Resources" of Akita University. The authors would like to thank the two anonymous journal reviewers who greatly improved the manuscript and Prof. Ildrem Syafri for his editorial handling.

References

Amma-Miyasaka, M. and Nakagawa, M., 2003. Evolution of deeper basaltic and shallower andesitic magmas during the AD 1469–1983 eruptions of Miyake-Jima Volcano, Izu–Mariana arc: inferences from temporal variations of mineral compositions in crystal-clots. *Journal of Petrology*, 44 (12), p.2113-2138. DOI: 10.1093/petrology/egg072.

Andi Mangga, S., Amirudin, Suwarti, T., Gafoer, S., and Sidarto, 1994. *Geology of the Tanjungkarang Quadrangle, Sumatra*. Geo-

logical Research and Development Centre, Bandung, p.19.

Barber, A.J., Crow, M.J., and Milsom, J. (eds.), 2005. *Sumatra: Geology, Resources and Tectonic Evolution*. Geological Society of London.

Belkin, H.E., Kilburn, C.R., and de Vivo, B., 1993. Sampling and major element chemistry of the recent (AD 1631-1944) Vesuvius activity. *Journal of Volcanology and Geothermal Research*, 58 (1-4), p.273-290. DOI: 10.1016/0377-0273(93)90113-6.

Bemmelen, R.W. Van, 1949. *The Geology of Indonesia*, Government Printing Office. Nijhoff, The Hague.

Borgia, A., Poore, C., Carr, M.J., Melson, W.G., and Alvarado, G.E., 1988. Structural, stratigraphic, and petrologic aspects of the Arenal-Chato volcanic system, Costa Rica: evolution of a young stratovolcanic complex. *Bulletin of Volcanology*, 50 (2), p.86-105. DOI: 10.1007/BF01275171.

Bronto, S., Asmoro, P., Hartono, G., and Sulistiyono, S., 2012. Evolution of Rajabasa Volcano in Kalianda Area and Its Vicinity, South Lampung Regency. *Indonesian Journal on Geoscience*, 7 (1), p.11-25. DOI: 10.17014/ijog.v7i1.132.

Camus, G., Gourgaud, A., and Vincent, P.M., 1987. Petrologic evolution of Krakatau (Indonesia): implications for a future activity. *Journal of Volcanology and Geothermal Research*, 33 (4), p.299-316. DOI: 10.1016/0377-0273(87)90020-5.

Carn, S.A. and Pyle, D.M., 2001. Petrology and geochemistry of the Lamongan Volcanic Field, East Java, Indonesia: primitive Sunda Arc magmas in an extensional tectonic setting?. *Journal of Petrology*, 42 (9), p.1643-1683. DOI: 10.1093/petrology/42.9.1643.

Dempsey, S., 2013. *Geochemistry of volcanic rocks from the Sunda Arc* (Doctoral dissertation, Durham University).

Fytikas, M. and Vougioukalakis, G., 1993. Volcanic structure and evolution of Kimolos and Polyegos (Milos Island group). *Bulletin of Geological Society of Greece*, 28, p.221-237.

Foden, J.D., 1983. The petrology of the calcalkaline lavas of Rindjani Volcano, east Sunda arc: a model for island arc petrogenesis. *Journal of Petrology*, 24 (1), p.98-130. DOI: 10.1093/petrology/24.1.98.

Gardner, M.F., Troll, V.R., Gamble, J.A., Gertisser, R., Hart, G.L., Ellam, R.M., Harris, C., and Wolff, J.A., 2012. Crustal differentiation processes at Krakatau volcano, Indonesia. *Journal of Petrology*, 54 (1), p.149-182. DOI: 10.1093/petrology/egs066.

Gerlach, D.C. and Grove, T.L., 1982. Petrology of Medicine Lake Highland volcanics: Characterization of endmembers of magma mixing. *Contributions to Mineralogy and Petrology*, 80 (2), p.147-159. DOI: 10.1007/BF00374892.

Gertisser, R. and Keller, J., 2000. The geochemical evolution of Merapi Volcano (Central Java): medium-K and high-K associations. *Abstract IAVCEI General Assembly, Bali*, p.150.

Gertisser, R. and Keller, J., 2003. Temporal variations in magma composition at Merapi Volcano (Central Java, Indonesia): magmatic cycles during the past 2,000 years of explosive activity. *Journal of Volcanology and Geothermal Research*, 123 (1-2), p.1-23. DOI: 10.1016/S0377-0273(03)00025-8.

Ghiorso, M.S. and Sack, R.O., 1995. Chemical mass transfer in magmatic processes IV. A revised and internally consistent thermodynamic model for the interpolation and extrapolation of liquid-solid equilibria in magmatic systems at elevated temperatures and pressures. *Contributions to Mineralogy and Petrology*, 119 (2-3), p.197-212. DOI: 10.1007/BF00307281.

Gill, R., 2010. *Igneous rocks and processes: a practical guide*. John Wiley & Sons.

Grove, T.L., Baker, M.B., and Kinzler, R.J., 1984. Coupled CaAl-NaSi diffusion in plagioclase feldspar: Experiments and applications to cooling rate speedometry. *Geochimica et Cosmochimica Acta*, 48 (10), p.2113-2121. DOI: 10.1016/0016-7037(84) 90391-0.

Gualda, G.A., Ghiorso, M.S., Lemons, R.V., and Carley, T.L., 2012. Rhyolite-MELTS: a modified calibration of MELTS optimized for silica-rich, fluid-bearing magmatic systems. *Journal of Petrology*, 53 (5), p.875-890. DOI: 10.1093/petrology/egr080.

Hall, R., 2009. Indonesia, geology. *Encyclopedia of Islands, University California Press, Berkeley, California*, p.454-460.

Harjono, H., Diament, M., Dubois, J., Larue, M., and Zen, M.T., 1991. Seismicity of the Sunda Strait: evidence for crustal extension and volcanological implications. *Tectonics*, 10 (1), p.17-30. DOI: 10.1029/90TC00285.

Hasibuan, R.F., 2014. *Geologi dan studi distribusi rekahan pada batuan vulkanik kuarter Gunung Rajabasa dan sekitarnya, Kabupaten Lampung Selatan, Provinsi Lampung* (Undergraduate Thesis, Institute of Technology, Bandung). DOI:10.25041/cepalo.v2no1.1763

Higgins, M.D., Voos, S., and Vander Auwera, J., 2015. Magmatic processes under Quizapu Volcano, Chile, identified from geochemical and textural studies. *Contributions to Mineralogy and Petrology*, 170 (5-6), p.51. DOI:10.1007/s00410-015-1209-5

Huchon, P. and Le Pichon, X., 1984. Sunda Strait and central Sumatra fault. *Geology*, 12 (11), p.668-672. DOI:10.1130/0091-7613(1984)12<668:SSACSF>2.0. CO;2.

Humphreys, M.C., Blundy, J.D., and Sparks, R.S.J., 2006. Magma evolution and open-system processes at Shiveluch Volcano: Insights from phenocryst zoning. *Journal of Petrology*, 47 (12), p.2303-2334. DOI: 10.1093/petrology/egl045.

Innocenti, S., del Marmol, M.A., Voight, B., Andreastuti, S., and Furman, T., 2013. Textural and mineral chemistry constraints on evolution of Merapi Volcano, Indonesia. *Journal of Volcanology and Geothermal Research*, 61, p.20-37. DOI: 10.1016/j.jvolgeores.2013.01.006.

Itaya, T., Nagao, K., Inoue, K., Honjou, Y., Okada, T., and Ogata, A., 1991. Argon isotope analysis by a newly developed mass spectrometric system for K–Ar dating. *Mineralogical Journal*, 15 (5), p.203-221. DOI: 10.2465/minerj.15.203.

Le Bas, M., Maitre, R.L., Streckeisen, A., Zanettin, B., and IUGS Subcommission on the Systematics of Igneous Rocks, 1986. A chemical classification of volcanic rocks based on the total alkali-silica diagram. *Journal of Petrology*, 27 (3), p.745-750. DOI: 10.1093/petrology/27.3.745.

Le Maitre, R.W., Bateman, P., Dudek, A., Keller, J., Lameyre, J., Le Bas, M.J., Sabine, P.A., Schmid, R., Sorensen, H., Streckeisen, A., and Woolley, A.R., 1989. *A classification of igneous rocks and glossary of terms. Recommendations of the IUGS Subcommission on the Systematics of Igneous rocks*. London: Blackwell Scientific Publications.

Malod, J.A., Karta, K., Beslier, M.O., and Zen Jr., M.T., 1995. From normal to oblique subduction: Tectonic relationships between Java and Sumatra. *Journal of Southeast Asian Earth Sciences*, 12 (1-2), p.85-93. DOI: 10.1016/0743-9547(95)00023-2.

McCaffrey, R., 1991. Slip vectors and stretching of the Sumatran fore arc. *Geology*, 1 (9), p.881-884. DOI: 10.1130/0091-7613(1991)019<0881:SVASOT>2.3.CO;2.

Métrich, N., Vidal, C.M., Komorowski, J.C., Pratomo, I., Michel, A., Kartadinata, N., Prambada, O., Rachmat, H., and Surono, 2017. New Insights into Magma Differentiation and Storage in Holocene Crustal Reservoirs of the Lesser Sunda Arc: the Rinjani–Samalas Volcanic Complex (Lombok, Indonesia). *Journal of Petrology*, 58 (11), p.2257-2284. DOI: 10.1093/petrology/egy006.

Miyashiro, A., 1974. Volcanic rock series in island arcs and active continental margins. *American Journal of Science*, 274 (4), p.321-355. DOI: 10.2475/ajs.274.4.321.

Morse, S.A., 1984. Cation diffusion in plagioclase feldspar. *Science*, 225 (4661), p.504-505. DOI: 10.1126/science.225.4661.504.

Nagao, K. and Itaya, T., 1988. K-Ar age determination. *Memoir of Geological Society of Japan*, 29, p.521.

Nagao, K., Nishido, H., Itaya, T., and Ogata, K., 1984. An age determination by K-Ar method. *Bulletin of the Hiruzen Research Institute,* Okayama University of Science, 9, p.19−38.

Nakamura, M. and Shimakita, S., 1998. Dissolution origin and syn-entrapment compositional change of melt inclusion in plagioclase. *Earth and Planetary Science Letters*, 161 (1-4), p.119-133. DOI: 10.1016/S0012-821X(98)00144-7.

Nazarwin., 1994. *Laporan Pemantauan Gunung Api Rajabasa dan Tinjauan Aspek-Aspek Geologinya di Daerah Kabupaten Lampung Selatan, Propinsi Lampung*, Kantor Wilayah Departemen Pertambangan dan Energi Provinsi Sumatra Selatan, Palembang. DOI:10.14710/jwl.6.1.58-73

Nelson, S.T. and Montana, A., 1992. Sieve-textured plagioclase in volcanic rocks produced by rapid decompression. *American Mineralogist*, 77 (11-12), p.1242-1249.

Newhall, C.G., 1979. Temporal variation in the lavas of Mayon Volcano, Philippines. *Journal of Volcanology and Geothermal Research*, 6 (1-2), p.61-83. DOI: 10.1016/0377-0273(79)90047-7.

Nier, A.O., 1950. A redetermination of the relative abundances of the isotopes of carbon, nitrogen, oxygen, argon, and potassium. *Physical Review*, 77 (6), p.789-793. DOI: 10.1103/PhysRev.77.789.

Ninkovich, D., 1976. Late Cenozoic clockwise rotation of Sumatra. *Earth and Planetary Science Letters*, 29 (2), p.269-275. DOI: 10.1016/0012-821X(76)90130-8.

Nishimura, S., 1980. Geological survey around Krakatau, Indonesia (1). *Tsukumo Earth Science, Kyoto Univ*, 15, p.1−10.

Nishimura, S., Abe, E., Nishida, J.I., Yokoyama, T., Dharma, A., Hehanussa, P., and Hehuwat, F., 1984. A gravity and volcanostratigraphic interpretation of the Lake Toba region, North Sumatra, Indonesia. *Tectonophysics*, 109 (3-4), p.253-272. DOI: 10.1016/0040-1951(84)90144-6.

Nishimura, S., Nishida, J.I., Yokoyama, T., and Hehuwat, F., 1986. Neo-tectonics of the Strait of Sunda, Indonesia. *Journal of Southeast Asian Earth Sciences*, 1 (2), p.81-91. DOI: 10.1016/0743-9547(86)90023-1.

Norini, G., Groppelli, G., Capra, L., and De Beni, E., 2004. Morphological analysis of Nevado de Toluca volcano (Mexico): new insights into the structure and evolution of an andesitic to dacitic stratovolcano. *Geomorphology*, 62 (1-2), p.47-61. DOI: 10.1016/j.geomorph.2004.02.010.

Pe-Piper, G., Piper, D.J., and Perissoratis, C., 2005. Neotectonics and the Kos Plateau Tuff eruption of 161 ka, South Aegean arc. *Journal of Volcanology and Geothermal Research*, 139 (3-4), p.315-338. DOI: 10.1016/j.jvolgeores.2004.08.014.

Piper, D.J.W. and Perissoratis, C., 2003. Quaternary neotectonics of the South Aegean arc. *Marine Geology*, 198 (3-4), p.259-288. DOI: 10.1016/S0025-3227(03)00118-X.

Prosser, J.T. and Carr, M.J., 1987. Poás volcano, Costa Rica: geology of the summit region and spatial and temporal variations among the most recent lavas. *Journal of Volcanology and Geothermal Research*, 33 (1-3), p.131-146. DOI: 10.1016/0377-0273(87)90057-6.

Reubi, O. and Nicholls, I.A., 2004. Variability in eruptive dynamics associated with caldera collapse: an example from two successive eruptions at Batur volcanic field, Bali, Indonesia. *Bulletin of Volcanology*, 66 (2), p.134-148. DOI: 10.1007/s00445-003-0298-6.

Steiger, R. and Jäger, E., 1977. Subcommission on geochronology: convention on the use of decay constants in geo-and cosmochronology. *Earth and Planetary Science Letters*, 36 (3), p.359-362. DOI: 10.1016/0012-821X(77)90060-7.

Suswati, Haerani, N., and Sutawidjaja, I. S., 2001. Laporan Pemetaan Geologi Gunung

Api Rajabasa, Lampung. Pusat Vulkanologi dan Mitigasi Bencana Geologi (PVMBG), No. 05-2517-L, 72 (Unpublished).

Takahashi, R. and Nakagawa, M., 2015. Evolution and eruption processes of a highly porphyritic silicic magma system: Petrology of the historical eruptive stage of Hokkaido-Komagatake Volcano, Japan. *Journal of Petrology*, 56 (6), p.1089-1112. DOI: 10.1093/petrology/egv030.

Toya, N., Ban, M., and Shinjo, R., 2005. Petrology of Aoso Volcano, northeast Japan arc: temporal variation of the magma feeding system and nature of low-K amphibole andesite in the Aoso-Osore volcanic zone. *Contributions to Mineralogy and Petrology*, 148 (5), p.566-581. DOI: 10.1007/s00410-004-0621-z.

Tsuchiyama, A., 1985. Dissolution kinetics of plagioclase in the melt of the system diopside-albite-anorthite, and origin of dusty plagioclase in andesites. *Contributions to Mineralogy and Petrology*, 89 (1), p.1-16. DOI: 10.1007/BF01177585.

Tsukui, M., 1985. Temporal variation in chemical composition of phenocrysts and magmatic temperature at Daisen Volcano, southwest Japan. *Journal of Volcanology and Geothermal Research*, 26 (3-4), p.317336. DOI: 10.1016/0377-0273(85)90062-9.

Villemant, B., Trigila, R. and DeVivo, B., 1993. Geochemistry of Vesuvius volcanics during 1631–1944 period. *Journal of Volcanology and Geothermal Research*, 58 (1-4), p.291-313. DOI: 10.1016/0377-0273(93)90114-7.

Wibowo, H.E., 2017. *Petrological and Geochemical Study of Sundoro Volcano, Central Java, Indonesia: Temporal Variation in Differentiation and Source Processes in the Growth of an Individual Volcano* (Doctoral dissertation, Hokkaido University).

Yagi, K., 2006. Manual of mineral separation for K-Ar age dating. *Engineering Geology of Japan, 0," The special issue of 10th anniversary of Hiruzen Institute for Geology and Chronology"*, p.19-25.